



# Construction of new enriched beam models accounting for cross-section deformation and pinching

Asma Bousselmi, Frej Chaouachi, J.F. Ganghoffer, Ali Zghal

## ► To cite this version:

Asma Bousselmi, Frej Chaouachi, J.F. Ganghoffer, Ali Zghal. Construction of new enriched beam models accounting for cross-section deformation and pinching. *International Journal of Mechanical Sciences*, 2019, 155, pp.488-508. 10.1016/j.ijmecsci.2019.02.046 . hal-03284078

**HAL Id: hal-03284078**

**<https://hal.univ-lorraine.fr/hal-03284078>**

Submitted on 22 Oct 2021

**HAL** is a multi-disciplinary open access archive for the deposit and dissemination of scientific research documents, whether they are published or not. The documents may come from teaching and research institutions in France or abroad, or from public or private research centers.

L'archive ouverte pluridisciplinaire **HAL**, est destinée au dépôt et à la diffusion de documents scientifiques de niveau recherche, publiés ou non, émanant des établissements d'enseignement et de recherche français ou étrangers, des laboratoires publics ou privés.



Distributed under a Creative Commons Attribution - NonCommercial 4.0 International License

## Construction of new enriched beam models accounting for cross-section deformation and pinching

<sup>a</sup>Asma Bousselmi, <sup>a</sup>Frej Chaouachi, <sup>b</sup>Jean-François Ganghoffer, <sup>a</sup>Ali Zghal

<sup>a</sup>Unité de recherche de mécanique des solides, structures et développements technologiques. ENSIT. Université de Tunis, BP56, Bab Mnara 1008, Tunisie

<sup>b</sup>LEM3 - CNRS. Université de Lorraine. 7, rue Félix Savart. 57073 Metz, France

### Abstract

The consideration of nonclassical beam theories beyond Timoshenko beam model is necessary in applications involving complex yarns subjected to transverse compaction, for which the section dilatation and in-plane shear require a detailed kinematic and static modeling. In the present work, new enriched beam elements with additional degrees of freedom are derived from the mechanics of generalized continua, allowing a representation of the in plane-shear and dilatation of sections. As a novel aspect, enriched beam model called microdilatation, macroshear, and macrostrain have been constructed on the basis of generalized beam theories but with a more condensed kinematics, assuming uniform hyperstress tensor within the beam. The choice of the adequate extended continuum for a given beam depends on its macroscopic deformation mechanisms. As a result, the developed beam models include modified material parameters (the tensile, shear and bulk moduli for an isotropic beam) involving additional microstructural parameters. These macrobeam models are expected to better describe the in plane-shear and dilatation of the beam sections along its mean line in comparison to classical beam theories. Numerical illustrative examples show that the microdilatation beam model has the ability to capture the local deformation field around holes, in contrast to Timoshenko beam model. The parameters of the microdilatation beam model provide a very good estimate of the overall porosity.

**Key words:** enriched beam models; finite deformations; cross-section deformation; pinching; beam macro-continua; generalized continua; model reduction

### 1. Introduction

Beam theories are all based on simplifying assumptions, since a full 3D model including all deformation modes in the context of finite strains is still challenging nowadays and no unitary view yet exists. The classical, most frequently employed theory is the Euler–Bernoulli beam theory [3] tracing back to the middle of the eighteen century (Bernoulli, 1751; Euler, 1744), relying on the hypothesis that the cross-section remains perpendicular to the beam centerline after deformation. Adding to this model the inextensibility constraint leads to Kirchhoff model (Kirchhoff, 1876) [4]. Unlike those models, the Timoshenko beam theory (Timoshenko, 1921, 1922) [1] allows for a rotation between the cross-section and the beam axis with a uniform shear distribution along the cross-section of the beam, which by hypothesis behaves as a rigid body in its own plane. Many methods have been proposed to overcome these limitations by means of different approaches: shear correction factors, warping functions based on the de Saint-Venant’s solution, the variational asymptotic solution, generalized beam theories. Recent developments in beam models have been made by Gruttmann [26] to evaluate shear correction factors. El Fatmi [27] improved the displacement models by introducing a warping function. Berdichevsky [28] proposed an Asymptotic-type expansion on the basis of variational methods. Carrera [29] introduce a beam model based on automatic techniques to build governing equations and/or

finite element matrices. The resulting theories permit one to deal with any section geometries subjected to any loading.

None of these theories can however detect non-classical effects such as warping, or out- and in-plane deformations; these phenomena are important for thick beams undergoing large motions, in applications involving complex yarns subjected to transverse compaction, like electric wires, multifilamentary structures in technical textiles, submarine cables, or ligaments and muscles in the context of biomechanics.

A beam is considered as a continuous body with a constrained position field, which is described by the motion of a centerline and the motion of planar cross-sections attached to every point of the centerline (fig. 1). For classical beams (Euler-Bernoulli, Timoshenko), a triad of rigid directors  $\mathbf{d}_1(s), \mathbf{d}_2(s), \mathbf{d}_3(s)$  is attached to every material point (fig. 1), and such a model can be considered as a Cauchy medium. All classical beam theories including Euler-Bernoulli, Kirchhoff, and Timoshenko theories can be described regarding the parameterization of all material points by introducing a set of three orthonormal directors  $\mathbf{d}_1(s), \mathbf{d}_2(s), \mathbf{d}_3(s)$ , with the section spanned by the two vectors  $\mathbf{d}_1(s), \mathbf{d}_2(s)$  (fig. 1) which satisfy the following conditions

$$\mathbf{d}_\alpha(s) \cdot \mathbf{d}'_\alpha(s) = \delta_{ij}$$

The notation  $(.)'$  represents Euler-Bernoulli beam model, thereby making the additional kinematic assumption that the cross-sections remain orthogonal to the centerline; hence it holds the following additional kinematic constraint:

$$\mathbf{d}_3(s) = k\mathbf{r}'(s)$$

The even more specific case of Kirchhoff rods adds the constraint  $k = 1$ .

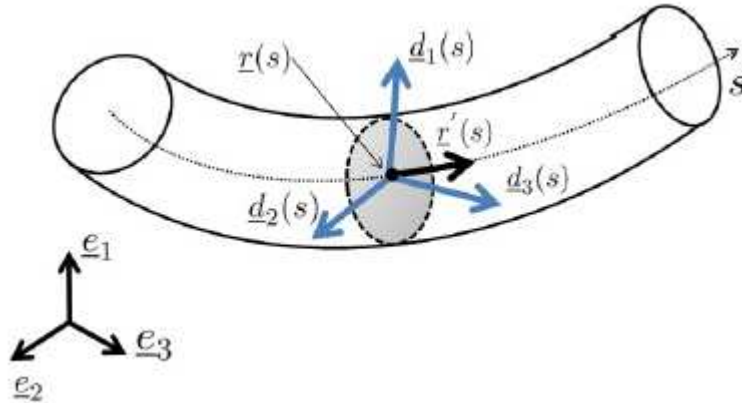


Figure 1: cross-section of a beam with the three directors in the deformed configuration [8]

These classical theories consider a rigid section, so that the directors can only rotate around the third director  $\mathbf{d}_3(s)$ . For generalized beams such as these introduced in this work, the triad of deformable directors is considered as deformable, thereby introducing extra degrees of freedom, thus going beyond Cauchy elasticity.

Complex yarns in 3D technical textiles are multifilamentary structures showing couplings between deformation modes; the yarns are especially subjected to the contact forces due to neighboring yarns leading to a compaction of the section, thus requiring the consideration of the section dilatation and in-plane shear. These motivations have driven the need for to develop enriched beam models, in order to account for all phenomena that have been neglected in the classical beam theories: this includes Poisson's effect quantified by the scalar quantity

$\frac{1}{2}(\mathbf{d}_\alpha(s) \cdot \mathbf{d}_\alpha(s) - 1)$  and the pinching effect represented by the term  $\frac{1}{2}\mathbf{d}_\alpha(s) \cdot \mathbf{d}'_\alpha(s)$ , which are respectively of first and second orders; there are in addition in-plane shear modes associated to

the quantity  $\frac{1}{2}\mathbf{d}_1(s).\mathbf{d}_2(s)$ . The usual method to build beam theories relies on the writing of the principle of virtual work, whereby one introduces conjugates strain and stress measures describing all deformation modes retained at the microscopic level. The consideration of these additional phenomena leads to an enriched kinematics leading to a generalized deformation (of tensor nature) associated to a microdeformation of any material point; this has led in the literature to the development of diverse generalized continua, including the micromorphic, microdilatation, microshear, microstrain, micropolar continua [10] ; the underlying kinematic assumptions for these generalized continua are (increasing the set of kinematic constraints from one medium to the next one) the existence of a full nonsymmetrical microdeformation tensor (micromorphic medium), a pure dilatation along the directors (microdilatation medium), pure shear of the directors (microshear medium), pure dilatation and pure shear (microstrain medium), and pure rigid body rotation of the directors (micropolar medium). These models introduce higher order strain and stress tensors of third order which complement the second order classical strain and stress tensors of the Cauchy continuum. Both large strain and small strain beam models have been built following this methodology.

In order to describe the full kinematics of any beam cross-section and especially the cross-section deformation, the classical beam models are insufficient as discussed in the introduction. As a consequence of this limitation on the kinematic field and to avoid these types of deficiencies, Antmann [5] proposed an enriched kinematical non linear beam model. In this model, beam cross-sections are described by means of three vector fields. In comparison with Antmann model, Kumar [6] proposed a novel approach for nonlinear, three dimensional deformation of beams in allowing in-plane cross-sectional deformations. This approach is based on the polar decomposition of the mapping expressing the directors versus the fixed Cartesian basis vectors.

The main objective of this work is to take into account the section dilatation and the in-plane shear occurring within thick beams. As a novel aspect developed in this work, we shall construct enriched beam model on the basis of generalized beam theories but with a more condensed kinematics; as a result, the developed models will involve additional microstructural parameters or modified parameters in comparison to classical beam theories.

The outline of the present contribution is as follows: we expose in section 2 the kinematic description of the introduced beam models, the elaboration of the Green-Lagrange strain tensor for the beam theories in a large deformation context, accounting for the section dilatation and the derivation of the weak and strong forms of equilibrium. Section 3 is devoted to the formulation of the newly developed macro continua, the constitutive equation of which nurturing thereafter the macrobeam models. We classify in section 4 the different generalized beam models and construct in section 5 the rigidity matrix of the linearized macrobeam model. A summary of the work and few perspectives of development are given in section 6.

## 2. Non-linear beam kinematics

In this section, we expose into details Antmann beam model in order to obtain the full Green-Lagrange strain tensor and the beam equilibrium equations.

### 2.1. Kinematic description

Referring to the theory of Antman [5], we describe the kinematics of the cross-section of a beam by three vectors field:  $\mathbf{r}(s)$  represents the position of the cross-section along the beam axis, while the two directors  $\mathbf{d}_\alpha(s)$  (not necessarily unit vectors or orthogonal vectors) lie in the

reference cross-section and allow evaluating the deformations occurring within the cross-section (Fig. 2).

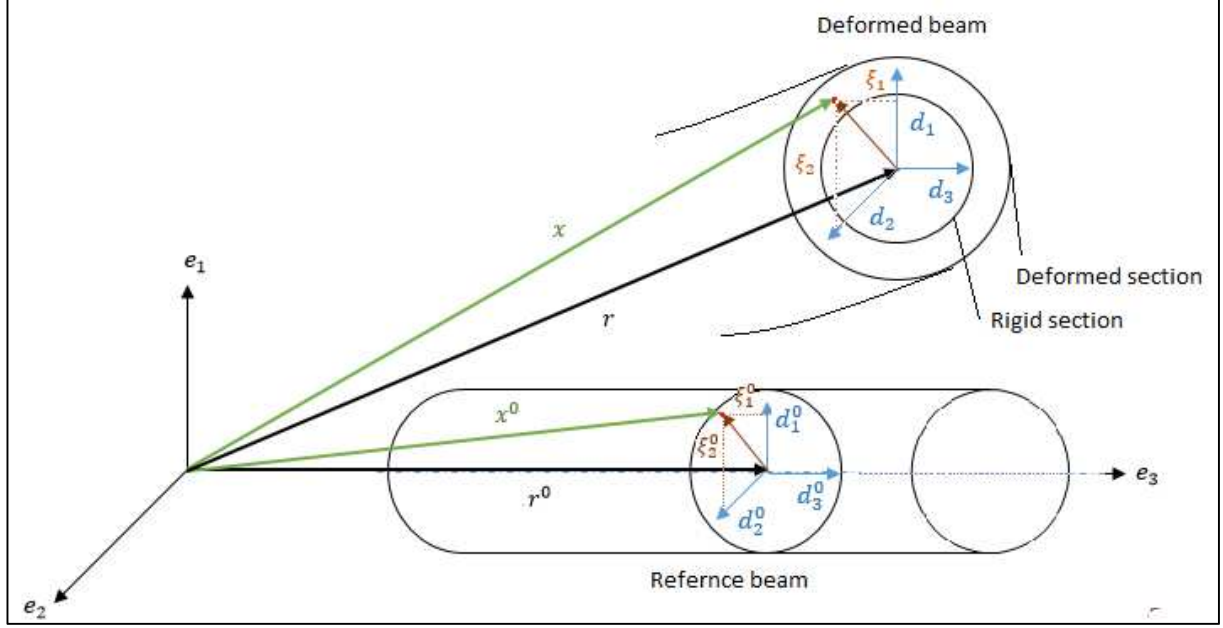


Figure 2: Geometric description of the beam in the reference and current configurations

The actual position of a material point in the actual configuration pictured in Fig. 1 writes

$$\mathbf{x}(\xi_1, \xi_2, s) = \mathbf{r}(s) + \sum_{\alpha=1}^2 \xi_{\alpha} \mathbf{d}_{\alpha}(s) \quad (1)$$

The vector  $\xi = (\xi_1, \xi_2)$  therein denotes the position of a generic material particle within the cross-section of the beam, so that  $\mathbf{x}$  is defined by the transverse coordinates  $(\xi_1, \xi_2)$  and the curvilinear abscissa  $s$  along the beam centerline. The general set of basis vectors  $\{\mathbf{d}_1, \mathbf{d}_2, \mathbf{d}_3\}$  is not orthonormal, so it holds:

$$\mathbf{d}_i \cdot \mathbf{d}_j \begin{cases} \neq 0 \text{ for } i \neq j \text{ (condition of non-orthogonality)} \\ \neq 1 \text{ for } i=j \text{ (condition of non-normality)} \end{cases} \quad (2)$$

The Green-Lagrange strain tensor for the Antmann beam model is computed from the previous motion; due to the fact the directors are not orthonormal, all the components are non nil a priori, thus it takes into account full three-dimensional effects. It writes after introducing equ. (2):

$$\mathbf{E} = \frac{1}{2} (\mathbf{F}^T \cdot \mathbf{F} - \mathbf{I}) \quad (3)$$

In (3), the dot denotes the inner product in the space of second order tensors; the deformation gradient in (3) writes in the present context based on (1) as:

$$\mathbf{F} = \underline{\mathbf{d}}_{\alpha} \otimes \underline{e}_{\alpha} + (\underline{\mathbf{r}}' + \xi_{\alpha} \underline{\mathbf{d}}_{\alpha}') \otimes \underline{e}_3 \quad (4)$$

The Green-Lagrange strain tensor can accordingly based on equ. (3) and (4) be written as:

$$\mathbf{E} = \begin{pmatrix} \frac{1}{2}(\mathbf{d}_1 \cdot \mathbf{d}_1) & (\mathbf{d}_1 \cdot \mathbf{d}_2) & (\mathbf{d}_1 \cdot \mathbf{r}') + \xi_2(\mathbf{d}_1 \cdot \mathbf{d}_2') + \xi_1(\mathbf{d}_1 \cdot \mathbf{d}_1') \\ (\mathbf{d}_1 \cdot \mathbf{d}_2) & (\mathbf{d}_2 \cdot \mathbf{d}_2) & (\mathbf{d}_2 \cdot \mathbf{r}') + \xi_1(\mathbf{d}_2 \cdot \mathbf{d}_1') + \xi_2(\mathbf{d}_2 \cdot \mathbf{d}_2') \\ (\mathbf{d}_1 \cdot \mathbf{r}') + \xi_2(\mathbf{d}_1 \cdot \mathbf{d}_2') + \xi_1(\mathbf{d}_1 \cdot \mathbf{d}_1') & (\mathbf{d}_2 \cdot \mathbf{r}') + \xi_1(\mathbf{d}_2 \cdot \mathbf{d}_1') + \xi_2(\mathbf{d}_2 \cdot \mathbf{d}_2') & \frac{1}{2}(\mathbf{r}' \cdot \mathbf{r}') + \xi_1(\mathbf{r}' \cdot \mathbf{d}_1') - \xi_2(\mathbf{r}' \cdot \mathbf{d}_2') \end{pmatrix} \quad (5)$$

We show in Table 1 the kinematic variables used in Antmann beam model and their physical meaning, thereby highlighting the mechanical significance of the components of the previously written Green-Lagrange strain tensor.

Antmann variables	Physical meaning of the introduced deformation variables
$\mathbf{d}_1 \cdot \mathbf{r}', \mathbf{d}_2 \cdot \mathbf{r}'$	Classical shear in directions $d_1(s)$ and $d_2(s)$
$\frac{1}{2} \mathbf{r}' \cdot \mathbf{r}'$	Traction-compression (bending line stretch)
$\mathbf{r}' \cdot \mathbf{d}_1', \mathbf{r}' \cdot \mathbf{d}_2'$	Bending
$\mathbf{d}_2 \cdot \mathbf{d}_1'$	Twist
$\frac{1}{2} \mathbf{d}_1 \cdot \mathbf{d}_1, \frac{1}{2} \mathbf{d}_2 \cdot \mathbf{d}_2$	cross-section dilatation
$\frac{1}{2} \mathbf{d}_1 \cdot \mathbf{d}_2$	in-plane shear
$\mathbf{d}_1 \cdot \mathbf{d}_1', \mathbf{d}_2 \cdot \mathbf{d}_2'$	pinching

Table 1: Antmann variables [5] and their physical meaning

## 2.2. Equilibrium equations

The beam equilibrium is written in weak form based on the virtual work principle, which states that the sum of the internal work of forces and the external work of applied forces vanishes. The internal virtual work writes:

$$\begin{aligned} P_{\text{int}} &= - \int_{\Omega_{\text{ref}}} \mathbf{S} : \hat{\mathbf{E}} d\Omega \\ &= \int_{\Omega_{\text{ref}}} (\mathbf{S}_0 + \xi_\alpha \mathbf{S}_\alpha) : (\hat{\mathbf{E}}_0 + \xi_\alpha \hat{\mathbf{E}}_\alpha) d\Omega \\ &= - \int_0^L \left\{ \underbrace{\mathbf{S}_0 : \hat{\mathbf{E}}_0}_{\text{A}} \left( \int_A dA \right) + \underbrace{(\mathbf{S}_0 : \hat{\mathbf{E}}_\alpha + \mathbf{S}_\alpha : \hat{\mathbf{E}}_0)}_0 \left( \int_A \xi_\alpha dA \right) + \underbrace{\mathbf{S}_\alpha : \hat{\mathbf{E}}_\alpha}_{\text{I}} \left( \int_A \xi_\alpha \xi_\phi dA \right) \right\} ds \end{aligned} \quad (6)$$

in which  $\mathbf{S}$  denotes the second Piola-Kirchhoff stress tensor, and the hat denotes a virtual kinematic field, defined as the variation of the total Lagrangian strain, thus it holds  $\hat{\mathbf{E}} = \delta \mathbf{E}$ . The internal virtual work takes the final form of a line integral over the beam centerline:

$$P_{\text{int}} = - \int_0^L \left\{ A(s) \mathbf{S}_0(s) : \hat{\mathbf{E}}_0(s) + \mathbf{S}_\alpha : \hat{\mathbf{E}}_\alpha I_{\alpha\beta} \right\} ds \quad (7)$$

This leads after some rearrangements to the following line integral with quantities therein factors of the kinematics described by the set of vectors  $\hat{\mathbf{r}}', \hat{\mathbf{d}}_1, \hat{\mathbf{d}}_2, \hat{\mathbf{d}}_1', \hat{\mathbf{d}}_2'$ :

$$P_{\text{int}}(\hat{x}) = - \int_0^L \left\{ -\mathbf{N}_{\text{int}} \cdot \hat{\mathbf{r}}' + \mathbf{G}_{\alpha, \text{int}} \cdot \hat{\mathbf{d}}_\alpha + \mathbf{H}_{\alpha, \text{int}} \cdot \hat{\mathbf{d}}_\alpha' \right\} ds \quad (8)$$

The prime therein denotes the derivative with respect to the curvilinear abscissa along the beam.

In (8), the classical and generalized efforts can indeed be written as:

$$\begin{aligned} \mathbf{N}_{\text{int}} &= \int_A (\mathbf{P} \cdot \mathbf{e}_3) \cdot dA \\ \mathbf{H}_{\alpha, \text{int}} &= \int_A \xi_\alpha (\mathbf{P} \cdot \mathbf{e}_3) \cdot dA \\ \mathbf{G}_{\alpha, \text{int}} &= \int_A (\mathbf{P} \cdot \mathbf{e}_\alpha) \cdot dA \end{aligned} \quad (9)$$

The vector  $\mathbf{N}_{\text{ext}}$  in previous expression represents the line density of forces acting on the beam cross-section while the vectors  $\mathbf{H}_{\alpha, \text{int}}$  and  $\mathbf{G}_{\alpha, \text{ext}}$  do not have any physical significance, as mentioned in [1] and [8]. To deal with this problem some works [6] propose the polar decomposition of the transformation gradient  $\mathbf{F}(s) = \mathbf{R}(s)\mathbf{U}(s)$ , with  $\mathbf{R}(s)$ ,  $\mathbf{U}(s)$  respectively the rotation of the beam cross-section and the pure deformation. So the actual position of a material point in the actual configuration writes :

$$\mathbf{x}(\xi_1, \xi_2, s) = \mathbf{r}(s) + \sum_{\alpha=1}^2 \xi_\alpha \mathbf{d}_\alpha(s) = \mathbf{r}(s) + \xi_\alpha \mathbf{R}(s)\mathbf{U}(s)e_\alpha \quad (10)$$

Let vector  $\xi$  denote the position of a generic material particle within the cross-section of the beam. Each director  $\mathbf{d}_\alpha(s)$  is mapped from the Cartesian basis vector from the product of a rigid body rotation  $\mathbf{R}$  and an in-plane cross-sectional deformation  $\mathbf{U}$ , as shown in figure 2:

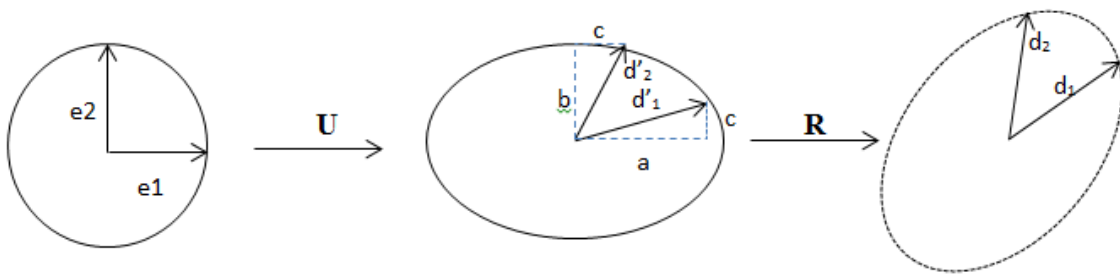


Figure 3: beam cross-section in-plane cross-sectional deformation followed by a rigid rotation

The internal virtual work writes:

$$P_{\text{int}} = - \int_{\Omega_{\text{ref}}} \mathbf{P} : \mathbf{F}' d\Omega = - \int_0^L \left\{ \begin{aligned} &\mathbf{R} \cdot \hat{\mathbf{v}} \cdot \int_A (\mathbf{P} \cdot \mathbf{e}_3) \cdot dA \\ &+ \mathbf{R} \cdot \hat{\mathbf{k}} \cdot \int_A \xi_\alpha \mathbf{R} \cdot \mathbf{U} e_\alpha \cdot (\mathbf{P} \cdot \mathbf{e}_3) \cdot dA \\ &+ \hat{\mathbf{U}}' \cdot \int_A \xi_\alpha \mathbf{e}_\alpha (\mathbf{R}^T \mathbf{P} \cdot \mathbf{e}_3) \cdot dA \\ &+ \hat{\mathbf{U}} \cdot \int_A \mathbf{e}_\alpha (\mathbf{R}^T \mathbf{P} \cdot \mathbf{e}_\alpha) \cdot dA \end{aligned} \right\} ds \quad (11)$$

in which the dot denotes a time derivative. Expression (11) can be rewritten in compact form as

$$P_{\text{int}} = - \int_0^L \left\{ \mathbf{N}_{\text{int}} \cdot \mathbf{R} \cdot \hat{\mathbf{v}} + \mathbf{M}_{\text{int}}^* \cdot \mathbf{R} \cdot \hat{\mathbf{k}} + \mathbf{Q}_{\alpha, \text{int}} \cdot \hat{\mathbf{U}}' + \mathbf{q}_{\alpha, \text{int}} \cdot \hat{\mathbf{U}} \right\} ds \quad (12)$$

Introducing therein classical efforts, moments and generalized efforts as follows

$$\mathbf{N}_{\text{int}} = \int_A (\mathbf{P} \cdot \mathbf{e}_3) \cdot dA \quad (13)$$

$$\mathbf{M}_{\text{int}}^* = \int_A \xi_\alpha \mathbf{R} \cdot \mathbf{U} e_\alpha \cdot (\mathbf{P} \cdot \mathbf{e}_3) \cdot dA \quad (14)$$

$$\mathbf{Q}_{\alpha, \text{int}} \approx \int_A \xi_\alpha \mathbf{e}_\alpha (\mathbf{R}^T \mathbf{P} \cdot \mathbf{e}_3) \cdot dA \quad (15)$$

$$\mathbf{q}_{\alpha, \text{int}} \approx \int_A \mathbf{e}_\alpha (\mathbf{R}^T \mathbf{P} \cdot \mathbf{e}_\alpha) \cdot dA \quad (16)$$

The external forces can further be introduced into the virtual work of external forces,

$$P_{\text{ext}} = \int_0^L \left\{ \mathbf{N}_{\text{ext}} \cdot \mathbf{R} \cdot \hat{\mathbf{v}} + \mathbf{M}_{\text{ext}} \cdot \mathbf{R} \cdot \hat{\mathbf{k}} + \mathbf{Q}_{\alpha, \text{ext}} \cdot \hat{\mathbf{U}} \right\} ds$$

Basing on the previous expressions of the internal and external virtual work, the equilibrium equations can then be written in the following global virtual form:

$$\mathbf{N}_{\text{int}}' + \mathbf{N}_{\text{ext}} = 0 \quad (17)$$

$$\mathbf{M}_{\text{int}}' + \mathbf{M}_{\text{ext}} = 0 \quad (18)$$

$$\mathbf{Q}_{\alpha, \text{int}}' - \mathbf{q}_{\alpha, \text{int}} + \mathbf{Q}_{\alpha, \text{ext}} = 0 \quad (19)$$

To simplify the resolution  $\mathbf{Q}_{\alpha, \text{int}}'$  can be neglected [6] by assuming that there is not much of nonuniformity in the cross-section. So the equ(19) can be reduced to equ (20):

$$-\mathbf{q}_{\alpha, \text{int}} + \mathbf{Q}_{\alpha, \text{ext}} = 0 \quad (20)$$

In the next section, we formulate the new macro-continua that will be used in the elaboration of the stress tensor.

### 3. Elaboration of beam macro-continua

In classical continuum mechanics, every material particle has three DOFs associated to translation and described by a position vector identifying the location of each particle [9]. A




generalized continuum is built from particles which possess extra degrees of freedom [10], abbreviated as DOFs in the sequel; these additional DOFs reflect on a continuum level the impact of the existing microstructure.

The micromorphic continuum is considered as the most general continuum with 12 DOF: three translational degrees of freedom and nine degrees of freedom of the microstructure (rotation, shear, and dilatation). The micromorphic theory can be reduced to the microstrain medium with 9 DOF's if one eliminates the micro-rotation [11]. The microshear continuum has 8 DOFs, namely 3 in translation and 5 for the pure strain part [12]; it can be also called the “incompressible microstrain continuum“. The microstretch media possesses 7 DOFs, namely three translations, three rotations and one stretch; it can be reduced to the micro-dilatation continuum if we eliminate the micro-rotation or to the micropolar continuum if we consider only the microrotation DOF in addition to the three classical translation DOFs.

In the micromorphic medium, each material point is viewed as a continuum in itself; the microscopic deformation of each point is characterized by a micro deformation tensor which is a priori incompatible. There are accordingly in total 12 DOFs, which make the micromorphic theory very rich and applicable to a wide range of situations; the theory is in fact specialized according to the considered application, with the specialization being in general dictated by the microscopic features which are likely to markedly influence the macroscopic behavior. Very often, the model is simplified so as to consider only rotations and a uniform dilatation/contraction of the microscopic effective continuum: this theory deserves the name microstretch and has been developed by Eringen [12,13]. The more specific case of a continuum with translation and rotation DOFs is the Cosserat continuum, also coined the micropolar continuum; to each point, there is a local rigid triad of vectors attached, which can rotate independently from the displacement, thus these media have 6 DOFs. It is worth noticing that this theory was in fact the first micromorphic theory appearing in the Cosserat brothers in 1909 [14]; this theory has been abandoned during nearly 50 years, and witnessed a revival with the works of Günther [15] in 1958 followed by Mindlin [16] in 1964. Finally, the simplest micromorphic medium in terms of DOFs is the microdilatation medium, including four DOFs, namely 3 displacements and an isotropic microdilatation; this simplification was initiated by Cowin [17, 18], and pursued in another form in [18,19]. The microdilatation model has been more recently applied to the 3D behavior of porous media [20, 21].

A summary of the existing generalized continua is presented in Table 2, which includes the constitutive equations satisfied by the Cauchy stress and hyperstress tensors, as well as the balance of linear momentum.

Type of generalized continuum	Balance equations	Constitutive equations	Number of material constants
Microstrain 	$\sigma_{kl,l} = 0$ $S_{klm,m} + \sigma_{kl} - s_{kl} = 0$	$\sigma_{kl} = (\lambda^g \varepsilon_{rr} + g_1 e_{rr}) \delta_{kl} + 2\mu^g \varepsilon_{kl} + 2g_2 e_{kl}$ $s_{kl} = (g_1 \varepsilon_{rr} + b_1 e_{rr}) \delta_{kl} + 2g_2 \varepsilon_{kl} + 2b_2 e_{kl}$ $S_{klm} = \tau_1 (\xi_{mrr} \delta_{kl} + \xi_{rrk} \delta_{ml}) + \tau_2 (\xi_{rmr} \delta_{kl} + \xi_{rrl} \delta_{ml})$ $+ \tau_3 \xi_{rrm} \delta_{kl} + \tau_4 \xi_{krr} \delta_{ml} + \tau_5 (\xi_{rkr} \delta_{ml} + \xi_{lrr} \delta_{mk})$ $+ \tau_6 \xi_{rlr} \delta_{mk} + \tau_7 \xi_{klm} + \tau_8 (\xi_{lmk} + \xi_{mkl}) +$ $\tau_9 \xi_{kml} + \tau_{10} \xi_{lkm} + \tau_{11} \xi_{mlk}$	17


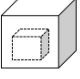
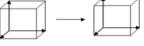
<b>Microshear</b> 		$\sigma_{kl} = (\lambda^g \varepsilon_{rr}) \delta_{kl} + 2\mu^g \varepsilon_{kl} + 2g_2 e_{kl}$ $s_{kl} = 2g_2 \varepsilon_{kl} + 2b_2 e_{kl}$ $S_{klm} = \tau_1 (\xi_{mrr} \delta_{kl} + \xi_{rrk} \delta_{ml}) + \tau_2 (\xi_{rmr} \delta_{kl} + \xi_{rrl} \delta_{ml})$ $+ \tau_3 \xi_{rrm} \delta_{kl} + \tau_4 \xi_{kr} \delta_{ml} + \tau_5 (\xi_{rkr} \delta_{ml} + \xi_{lrr} \delta_{mk})$ $+ \tau_6 \xi_{rlr} \delta_{mk} + \tau_7 \xi_{klm} + \tau_8 (\xi_{lmk} + \xi_{mkl}) +$ $\tau_9 \xi_{kml} + \tau_{10} \xi_{lkm} + \tau_{11} \xi_{mlk}$	15
<b>Micro-dilatation</b> 		$\sigma_{kl} = (\lambda^g \varepsilon_{rr} + g_1 e_{rr}) \delta_{kl} + 2\mu^g \varepsilon_{kl}$ $s_{kl} = (g_1 \varepsilon_{rr} + b_1 e_{rr}) \delta_{kl}$ $S_m = \tau_{12} e_{rr,m}$	5
<b>Cauchy</b> 	$\sigma_{kl,l} = 0$	$\sigma_{kl} = \lambda \varepsilon_{rr} \delta_{kl} + \mu (\varepsilon_{kl} + \varepsilon_{lk})$	2

Table 2: constitutive laws of the main classes of generalized continua

In Table 2,  $\sigma$  is the force stress tensor (a second order tensor),  $S$  the hyperstress tensor (a third order tensor),  $s$  the relative stress (a second order tensor) describing the coupling between  $\sigma$  and  $S$ , representing a penalty to strong deviations of the micromotion from the macromotion. The balance of linear momentum traducing the static equilibrium are written in the **Appendix 1** and will be used later on to construct the macro beam models.

We have here restricted for the clarity of the presentation to an isotropic behavior of the material, described by the two classical Lamé coefficients  $\lambda, \mu$  and the generalized Lamé coefficients  $\lambda^g, \mu^g$ .

The coefficients  $g_1, g_2, b_1, b_2, \tau_1, \tau_2, \tau_3, \tau_4, \tau_5, \tau_6, \tau_7, \tau_8, \tau_9, \tau_{10}, \tau_{11}, \tau_{12}$  appearing in the constitutive laws written in Table 2 are material parameters of the introduced generalized continua.

The classical constitutive laws are not capable of adequately describing the in-plane shear and cross-sectional beam deformations, due to the limited kinematics. We propose to introduce additional DOFs to every material particle of the beam centerline, leading in turn to generalized stress measures and constitutive laws.

The consideration of the full expressions of the generalized stress tensors for a beam includes more than one hundred generalized efforts (for the micromorphic continuum), thus leading to a very complicated beam model with many coefficients; in order to simplify the formulation, we shall propose new continua, less general than the full micromorphic continua, but still able to account for microstructural effects associated to the section deformation. Those new continua will be called “macro-continua” in the sequel. In these macro-continua, we will suppose that the hyper-stress is uniform since we are working on the scale of a single representative volume element; as a consequence, its divergence shall vanish, a condition was introduced into the previous equilibrium equations allows extracting the expressions of the relative deformation, which inserted into the expression of the stress tensor; technical details as to how this model reduction is done are exposed in the **Appendix 1**.

The resulting constitutive laws of the newly formulated continua are presented in Table 3.

Type of macrocontinuum	Number of material constants	Constitutive equations
Macrostrain	6	$\sigma_{kl} = \left( \lambda^g - \frac{g_1^2}{b_1} \right) \varepsilon_{rr} \delta_{kl} + \left( 2\mu^g - 2\frac{g_2^2}{b_2} \right) \varepsilon_{kl}$
Macroshear	4	$\sigma_{kl} = \left( \lambda^g \varepsilon_{rr} \right) \delta_{kl} + \left( 2\mu^g - 2\frac{g_2^2}{b_2} \right) \varepsilon_{kl}$
Macro dilatation	4	$\sigma_{kl} = \left( \lambda^g - \frac{g_1^2}{b_1} \right) \varepsilon_{rr} \delta_{kl} + 2\mu^g \varepsilon_{kl}$
Cauchy	2	$\sigma_{kl} = \lambda \varepsilon_{rr} \delta_{kl} + \mu (\varepsilon_{kl} + \varepsilon_{lk})$

Table 3: Constitutive laws of the introduced macro-continua

where  $\delta_{ij}$  is the Kronecker symbol. These macro-continua can have applications well beyond the present context of enriched beam models, typically for solids having a microstructure in a broad sense.

We next introduce in these integral the constitutive law of the enriched continuum (the two more specific macroshear and macro dilatation continua can be recovered as specific cases as mentioned in section 3) written in matrix format as:

$$\begin{pmatrix} \varepsilon_{11} \\ \varepsilon_{22} \\ \varepsilon_{33} \\ \varepsilon_{12} \\ \varepsilon_{13} \\ \varepsilon_{23} \end{pmatrix} = \begin{pmatrix} \Xi_1 & \Xi_2 & \Xi_2 & 0 & 0 & 0 \\ \Xi_2 & \Xi_1 & \Xi_2 & 0 & 0 & 0 \\ \Xi_2 & \Xi_2 & \Xi_1 & 0 & 0 & 0 \\ 0 & 0 & 0 & \Xi_3 & 0 & 0 \\ 0 & 0 & 0 & 0 & \Xi_3 & 0 \\ 0 & 0 & 0 & 0 & 0 & \Xi_3 \end{pmatrix} \begin{pmatrix} \sigma_{11} \\ \sigma_{22} \\ \sigma_{33} \\ \sigma_{12} \\ \sigma_{13} \\ \sigma_{23} \end{pmatrix} \quad (21)$$

$$\begin{pmatrix} \sigma_{11} \\ \sigma_{22} \\ \sigma_{33} \\ \sigma_{12} \\ \sigma_{13} \\ \sigma_{23} \end{pmatrix} = \begin{pmatrix} \Theta_1 & \Theta_2 & \Theta_2 & 0 & 0 & 0 \\ \Theta_2 & \Theta_1 & \Theta_2 & 0 & 0 & 0 \\ \Theta_2 & \Theta_2 & \Theta_1 & 0 & 0 & 0 \\ 0 & 0 & 0 & \Theta_3 & 0 & 0 \\ 0 & 0 & 0 & 0 & \Theta_3 & 0 \\ 0 & 0 & 0 & 0 & 0 & \Theta_3 \end{pmatrix} \begin{pmatrix} \varepsilon_{11} \\ \varepsilon_{22} \\ \varepsilon_{33} \\ \varepsilon_{12} \\ \varepsilon_{13} \\ \varepsilon_{23} \end{pmatrix} \quad (22)$$

with the matrix components therein expressed in Table 4.

Continuum	Matrix component	Expression
	$\Xi_1$	$\frac{b_2 (b_1 b_2 \lambda^g + b_1 b_2 \mu^g - b_1 g_2^2 - b_2 g_1^2)}{3b_1 b_2^2 \lambda^g \mu^g + 2b_1 b_2^2 \mu^{g^2} - 3b_1 b_2 g_2^2 \lambda^g - 4b_1 b_2 g_2^2 \mu^g + 2b_1 g_2^4 - 3b_2^2 g_1^2 \mu^g + 3b_2 g_1^2 g_2^2}$

Macrostrain	$\Xi_2$	$-\frac{1}{2} \frac{b_2^2 (b_1 \lambda^g - g_1^2)}{3b_1 b_2^2 \lambda^g \mu^g + 2b_1 b_2^2 (\mu^g)^2 - 3b_1 b_2 g_2^2 \lambda^g - 4b_1 b_2 g_2^2 \mu^g + 2b_1 g_2^4 - 3b_2^2 g_1^2 \mu^g + 3b_2 g_1^2 g_2^2}$
	$\Xi_3$	$\frac{1}{2} \frac{b_2}{b_2 \mu^g - g_2^2}$
	$\Theta_1$	$\lambda^g - \frac{g_1^2}{b_1} + 2\mu^g - 2 \frac{g_2^2}{b_2}$
	$\Theta_2$	$\lambda^g - \frac{g_1^2}{b_1}$
	$\Theta_3$	$2\mu^g - 2 \frac{g_2^2}{b_2}$
Macrosh ear	$\Xi_1$	$\frac{b_2 (b_2 \lambda^g + b_2 \mu^g - g_2^2)}{3b_2^2 \lambda^g \mu^g + 2b_2^2 (\mu^g)^2 - 3b_2 g_2^2 \lambda^g - 4b_2 g_2^2 \mu^g + 2g_2^4}$
	$\Xi_2$	$-\frac{1}{2} \frac{b_2^2 \lambda^g}{3b_2^2 \lambda^g \mu + 2b_2^2 \mu^2 - 3b_2 g_2^2 \lambda^g - 4b_2 g_2^2 \mu^g + 2g_2^4}$
	$\Xi_3$	$\frac{1}{2} \frac{b_2}{b_2 \mu^g - g_2^2}$
	$\Theta_1$	$\lambda^g + 2\mu^g - 2 \frac{g_2^2}{b_2}$
	$\Theta_2$	$\lambda^g$
	$\Theta_3$	$2\mu^g - 2 \frac{g_2^2}{b_2}$
Macro-dilatation	$\Xi_1$	$\frac{b_1 \lambda^g + b_1 \mu^g - g_1^2}{\mu^g (3b_1 \lambda^g + 2b_1 \mu^g - 3g_1^2)}$
	$\Xi_2$	$-\frac{1}{2} \frac{b_1 \lambda^g - g_1^2}{\mu^g (3b_1 \lambda^g + 2b_1 \mu^g - 3g_1^2)}$
	$\Xi_3$	$\frac{1}{2\mu^g}$
	$\Theta_1$	$\lambda^g - \frac{g_1^2}{b_1} + 2\mu^g$
	$\Theta_2$	$\lambda^g - \frac{g_1^2}{b_1}$

	$\Theta_3$	$2\mu^s$
--	------------	----------

Table 4: components of the constitutive law of generalized continuum

The new expressions of the tensile, Poisson ratio and shear elastic moduli – respectively the positive scalar quantities  $E, \nu, G$  - of the macro-continua introduced in Table 2 in the context of isotropic elasticity are given in Table 5.

Macrostrain continuum	
$E$	$\frac{3b_1b_2^2\lambda^s\mu^s + 2b_1b_2^2(\mu^s)^2 - 3b_1b_2g_2^2\lambda^s - 4b_1b_2g_2^2\mu^s + 2b_1g_2^4 - 3b_2^2g_1^2\mu^s + 3b_2g_1^2g_2^2}{(b_1b_2\lambda^s + b_1b_2\mu^s - b_1g_2^2 - b_2g_1^2)b_2}$
$\nu$	$\frac{1}{2} \frac{(b_1\lambda^s - g_1^2)b_2}{b_1b_2\lambda^s + b_1b_2\mu^s - b_1g_2^2 - b_2g_1^2}$
$G$	$\mu^s - \frac{g_2^2}{b_2}$
Macroshear continua	
$E$	$\frac{3b_2^2\lambda^s\mu^s + 3b_2^2(\mu^s)^2 - 3b_2g_2^2\lambda^s + 2g_2^4}{(b_2\lambda^s + b_2\mu^s - g_2^2)b_2}$
$\nu$	$\frac{1}{2} \frac{b_2\lambda^s}{b_2\lambda^s + b_2\mu^s - g_2^2}$
$G$	$\mu^s - \frac{g_2^2}{b_2}$
Macro dilatation continua	
$E$	$\frac{\mu^s(3b_1\lambda^s + 2b_1\mu^s - 3g_1^2)}{b_1\lambda^s + b_1\mu^s + g_1^2}$
$\nu$	$\frac{1}{2} \frac{b_1\lambda^s - g_1^2}{b_1\lambda^s + b_1\mu^s - g_1^2}$
$G$	$\mu^s$
Cauchy continua	
$E$	$\frac{\mu(3\lambda + 2\mu)}{\lambda + \mu}$
$\nu$	$\frac{1}{2} \frac{\lambda}{\lambda + \mu}$

$G$	$\mu$
-----	-------

Table 5: expressions of the elastic moduli of generalized continua

It is clear from the expressions of the elastic moduli of generalized continua given in Table 5 that the new nonclassical material constants will lead to different values of the set of effective properties  $E, G, \nu$  of the macrobeams; this will have an impact on the mechanical response of the beam equipped with these new properties, in comparison to a classical beam. One expects especially that the section dilatation will be modified due to the introduction of an enhanced set of mechanical properties of the macrobeams.

The expressions of the stress tensors of the formulated macrocontinua will be used in the next section to formulate new macro-beam models.

#### 4. Classification of the generalized beam models

In order to set the stage, a classification of some important beam models of the literature is recalled in Table 6. In the sequel, we shall concentrate on the construction of macro beam models; the wording macro is used to by analogy with the framework of continuous media used for the modeling of the beam kinematics.

The novel aspects considered in this contribution are the setting up of macrostretch and macrodilatation beam models, as pictured in Table 6, which provides the link between the micro-continua, the enriched beam theories with the underlying assumptions of the director motion, and (right column) the associated generalized beam models.

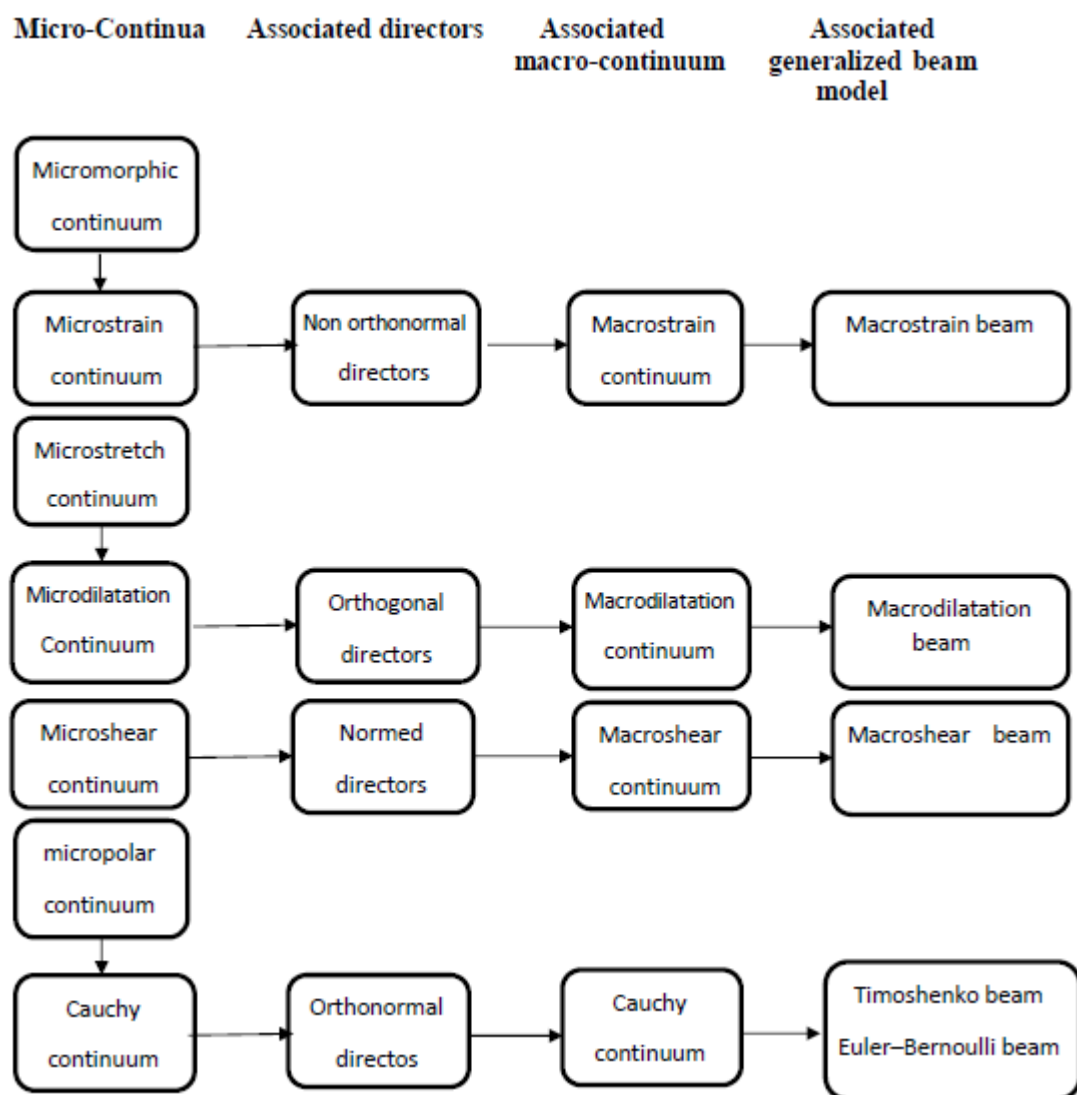
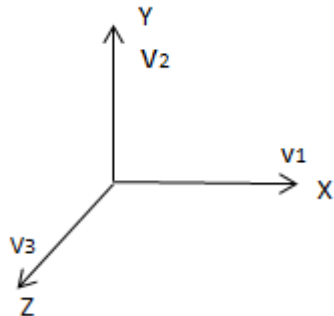
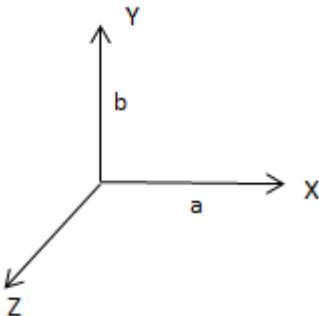


Table 6: classification of beam models based on reduction of the microcontinua

The aim of our work is to redefine every material point of the bending line of the beam. In classical theories the set of directors accorded to every point is rigid but in generalized continuum and beams those directors will be able to deform. In Table 7 we introduce the classical and generalized deformations.

Directors initial configuration	Directors deformed configuration	
	Directors rigid deformation	Directors non-rigid deformation
		

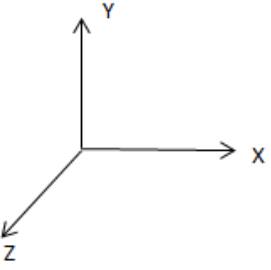
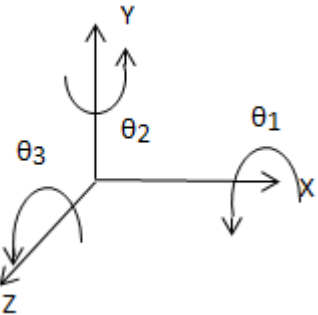
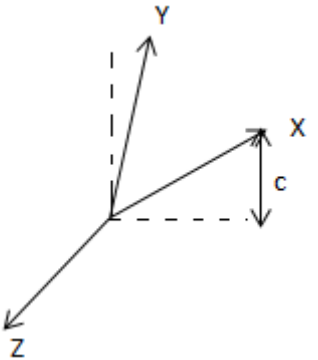
 <p>Orthonormal directors</p>	Translation	Dilatation of directors ( $a, b \neq 1$ )
	<p>Orthonormal directors</p>  <p>Rotation : Orthonormal directors</p>	<p>Orthogonal directors (non normed)</p>  <p>In plane shear: normed directors</p>

Table7: Directors in the initial and deformed configurations

We concentrate in this contribution on the development of macrobeam models. The kinematic assumptions underlying the macrobeam models in comparison to more classical beam models (including Euler-Bernoulli and Timoshenko beam theories) are exposed in Table 8.

	Shear deformation (existence of a rotation between the directors and the centerline)		Normality condition of the directors		Orthogonality condition of the directors	
	the principal director and the bending line remains collinear after bending	An angle appears between the principal director and the bending line	Normed directors	Non normed directors	Orthogonal directors	Non orthogonal directors
Euler-Bernoulli beam	✓		✓		✓	
Timoshenko beam		✓	✓		✓	
Macro dilatation beam	✓			✓	✓	
		✓		✓	✓	
Macro shear beam	✓		✓			✓
		✓	✓			✓
Macro strain beam	✓			✓		✓



		✓		✓		✓
--	--	---	--	---	--	---

Table 8: classification of the beam models according to the deformation of the beam directors

A summary of the main classes of beam models, the existing DOFs and their underlying assumptions is exposed in Table 9. The basic assumptions formulated in these models are the following:

H1: the cross-sections remain perpendicular to the bending line after deformation (no shear deformation).

H2: The sections remains plane after deformation (there is no warping).

H3: The directors are of unit norm, thus excluding Poisson effect (no cross-section dilatation).

H4: The directors are orthogonal (the in-plane shear deformations vanish).

Beam model	Number of DOFs	DOFs	Assumptions	References
Macrostrain beam	8	Translation	$H2$	-
	6	rotation dilatation in plane shear	$H2, H1$	Present work
Macroshear beam	7	Translation	$H2, H3$	-
	4	rotation in plane shear	$H1, H2, H3$	Present work
Macro dilatation beam	7	Translation	$H1, H2, H4$	-
	4	rotation dilatation	$H2, H4$	Present work
Timoshenko beam	6	Translation rotation	$H1, H2, H4$	Timoshenko (1922) [1]
Euler-Bernoulli beam	3	Translation rotation	$H1, H2, H3, H4$	Bernoulli (1751) Euler (1744)

Table 9: Synthetic presentation of the hierarchy of the obtained beam models.

The linearization of the formulated macrobeam continua is done in the next section, in order to evaluate their rigidity matrices.

## 5. Linearization and formulation of the macrobeam model

In this section we linearize the kinematics of the enriched beam and we establish the formulation of the macrobeam model.

### 5.1. Linearization of the kinematics

The linearization of the finite strain tensor is next performed, with the objective the determination of the stiffness matrices, relying on previous linearized quantities. Let start by decomposing the transformation gradient expressed in (4) and introducing therein its polar decomposition as follows:

$$\begin{aligned} \mathbf{F} &= \underline{\mathbf{d}}_\alpha \otimes \mathbf{e}_\alpha + (\mathbf{r}' + \xi_\alpha \underline{\mathbf{d}}_\alpha') \otimes \mathbf{e}_3 = \mathbf{R} \cdot \mathbf{U} \cdot \mathbf{e}_\alpha \otimes \mathbf{e}_\alpha + \left( \mathbf{r}' + \xi_\alpha (\mathbf{R}' \cdot \mathbf{U} + \mathbf{R} \cdot \mathbf{U}') \cdot \mathbf{e}_\alpha \right) \otimes \mathbf{e}_3 \\ \mathbf{F} &= \mathbf{R} \cdot \left[ \mathbf{U} \cdot \mathbf{e}_\alpha \otimes \mathbf{e}_\alpha + \left( \underbrace{\mathbf{R}^T \cdot \mathbf{r}'}_{\mathbf{v}} + \xi_\alpha \left( \underbrace{\mathbf{R}^T \cdot \mathbf{R}'}_{\mathbf{K}} \cdot \mathbf{U} + \mathbf{U}' \right) \cdot \mathbf{e}_\alpha \right) \otimes \mathbf{e}_3 \right] \end{aligned} \quad (23)$$

In previous expression, the shear and axial stretch were reflected by the vector  $\mathbf{v} = \mathbf{R}^T \cdot \mathbf{r}' = \begin{pmatrix} v_1 \\ v_2 \\ v_3 \end{pmatrix}$ ,

while the local curvature and twist are traduced by the antisymmetrical tensor  $\mathbf{K}$ . We further write the right Cauchy-Green tensor as follows

$$\begin{aligned} \mathbf{F}^T \cdot \mathbf{F} &= \mathbf{R} \cdot \left[ \mathbf{U} \cdot \mathbf{e}_\alpha \otimes \mathbf{e}_\alpha + \left( \underbrace{\mathbf{R}^T \cdot \mathbf{r}'}_{\mathbf{v}} + \xi_\alpha \left( \underbrace{\mathbf{R}^T \cdot \mathbf{R}'}_{\mathbf{K}} \cdot \mathbf{U} + \mathbf{U}' \right) \cdot \mathbf{e}_\alpha \right) \otimes \mathbf{e}_3 \right]^T \cdot \mathbf{R} \cdot \left[ \mathbf{U} \cdot \mathbf{e}_\alpha \otimes \mathbf{e}_\alpha + \left( \underbrace{\mathbf{R}^T \cdot \mathbf{r}'}_{\mathbf{v}} + \xi_\alpha \left( \underbrace{\mathbf{R}^T \cdot \mathbf{R}'}_{\mathbf{K}} \cdot \mathbf{U} + \mathbf{U}' \right) \cdot \mathbf{e}_\alpha \right) \otimes \mathbf{e}_3 \right] \\ &= \mathbf{U}^T \cdot \mathbf{U} \cdot (\mathbf{e}_\alpha \otimes \mathbf{e}_\alpha) + (\mathbf{e}_3 \otimes \mathbf{V}) \cdot (\mathbf{U} \cdot \mathbf{e}_\alpha \otimes \mathbf{e}_\alpha) + (\mathbf{U} \cdot \mathbf{e}_\alpha \otimes \mathbf{e}_\alpha) \cdot (\mathbf{e}_3 \otimes \mathbf{V}) + (\mathbf{V}^T \cdot \mathbf{V}) (\mathbf{e}_3 \otimes \mathbf{e}_3) \end{aligned} \quad (24)$$

The principal idea on which we base the linearization of the kinematics is to rely on the Green-Lagrange strain tensor expressed in (5), inserting therein the decomposition of the directors introduced in Kumar [6], viz

$$\underline{\mathbf{d}}_\alpha = \mathbf{R} \cdot \mathbf{U} \cdot \mathbf{e}_\alpha \quad (25)$$

The small strains tensors are obtained by linearizing the corresponding micromorphic beam large strain tensors in the previous Table. The pure deformation tensor in the polar decomposition of the transformation gradient simplifies to the identity tensor, whereas it is generalized in the

present enriched beam model to  $\mathbf{U} = \begin{bmatrix} a & c & 0 \\ c & b & 0 \\ 0 & 0 & 1 \end{bmatrix}$ , which gives after linearization

$$\mathbf{U} \equiv \begin{pmatrix} 1+\delta a & \delta c & 0 \\ \delta c & 1+\delta b & 0 \\ 0 & 0 & 1 \end{pmatrix} = \begin{pmatrix} 1 & 0 & 0 \\ 0 & 1 & 0 \\ 0 & 0 & 1 \end{pmatrix} + \underbrace{\begin{pmatrix} \delta a & \delta c & 0 \\ \delta c & \delta b & 0 \\ 0 & 0 & 0 \end{pmatrix}}_{\boldsymbol{\psi}} = \mathbf{I} + \boldsymbol{\psi} \quad (26)$$

with  $\boldsymbol{\psi}$  therein incremental pure deformation tensor, representing the small strains tensor, and  $\delta a, \delta b, \delta c$  the variations of the corresponding finite quantities  $a, b, c$  respectively. The rotation tensor is further linearized as (using the identity  $\mathbf{R}^T \cdot \mathbf{R} = \mathbf{I}$ )

$$\mathbf{R} \cong \mathbf{I} + \mathbf{w}, \quad \mathbf{w} + \mathbf{w}^T = \mathbf{0} \quad (27)$$

introducing therein the linearized antisymmetrical rotation tensor  $\mathbf{w}$ . This entails the antisymmetrical tensor

$$\mathbf{K} = \mathbf{R}^T \cdot \mathbf{R}' \cong \mathbf{w}' = \begin{pmatrix} 0 & k_3 & -k_2 \\ -k_3 & 0 & k_1 \\ k_2 & -k_1 & 0 \end{pmatrix} \quad (28)$$

We further linearize the vector, so it holds  $\mathbf{v} \cong \begin{pmatrix} 1 + v_1 \\ 1 + v_2 \\ 1 + v_3 \end{pmatrix}$ .

We resume in Table 10 the variables and their physical meanings:

	Variables	Physical meanings
Rigid deformations	$v_3, v_1, v_2$	translations on the axes z, x, y
	$k_3, k_1, k_2$	rotations around the axes z, x, y
Non-rigid deformations	$\delta a$	dilatation on the axe x
	$\delta b$	dilatation on the axe y
	$\delta c$	In plan shear variation
	$\delta a'$	Pinching angle
	$\delta b'$	Pinching angle
	$\delta c'$	Pinching angle

Table 10: Variables and their physical meanings

The linearized strain tensor is obtained using developments exposed in the **Appendix 2**:

$$\bar{\mathbf{E}} = \frac{1}{2} \begin{bmatrix} \delta a & \delta c & v_1 + \delta a + \delta c - \xi_2 k_2 + \xi_1 \delta a' \\ \delta c & \delta b & v_2 + \delta c + \delta b + \xi_1 k_2 + \xi_2 \delta b' \\ v_1 + \delta a + \delta c - \xi_2 k_2 + \xi_1 \delta a' & v_2 + \delta c + \delta b + \xi_1 k_2 + \xi_2 \delta b' & 2v_3 - \xi_1 k_3 + \xi_2 k_1 \end{bmatrix} \quad (29)$$

This linearized strain tensor shall be used in subsequent developments to establish the small strains stiffness matrix for the macrobeam continua.

## 5.2. Formulation of the macrobeam

The rigidity matrix relates the generalized force vector to the vector including the generalized DOFs); its derivation relies on the expansion of the work of internal forces, introducing the linearized strain tensor, as expanded in this section.

$$\begin{aligned}
w_i^* &= - \int_V \sigma^T \hat{\epsilon} dV \\
&= \left( \begin{aligned}
&\int_0^L \left( \int_s \underbrace{\sigma_{33}}_N dS \right) \hat{v}'_3 \\
&+ \int_0^L \left( \int_s \underbrace{\sigma_{31}}_{T_x} dS \right) (\hat{v}'_1 + \delta \hat{a} + \delta \hat{c}) + \int_0^L \left( \int_s \underbrace{\sigma_{32}}_{T_y} dS \right) (\hat{v}'_2 + \delta \hat{b} + \delta \hat{c}) \\
&+ \int_0^L \left( \int_s \underbrace{-\xi_1 \sigma_{33}}_{Mf_x} dS \right) \hat{k}'_3 + \int_0^L \left( \int_s \underbrace{\xi_2 \sigma_{33}}_{Mf_y} dS \right) \hat{k}'_1 \\
&+ \int_0^L \left( \int_s \underbrace{(\xi_2 \sigma_{31} - \xi_1 \sigma_{32})}_M dS \right) \hat{k}'_2 \\
&+ \int_0^L \left( \int_s \underbrace{\xi_1 \sigma_{31}}_{Q_1} dS \right) \delta \hat{a}' + \int_0^L \left( \int_s \underbrace{\xi_2 \sigma_{32}}_{Q_2} dS \right) \delta \hat{b}'
\end{aligned} \right) dz + \left( \begin{aligned}
&\left( \int_0^h \left( \int_{s_x} \underbrace{\sigma_{11}}_{q_{11}} dS_x \right) \delta \hat{a} + \right. \\
&\left. \int_0^h \left( \int_{s_x} \underbrace{\sigma_{12}}_{q_{12}} dS_x \right) \delta \hat{c} \right) dx \\
&+ \left( \int_0^b \left( \int_{s_y} \underbrace{\sigma_{22}}_{q_{22}} dS_y \right) \delta \hat{b} + \right. \\
&\left. + \int_0^b \left( \int_{s_x} \underbrace{\sigma_{12}}_{q_{12}} dS_y \right) \delta \hat{c} \right) dy
\end{aligned} \right) \quad (30)
\end{aligned}$$

We have introduced in (30) the hat as a overhead notation to denote the virtual kinematics; since the stress components act in different directions, one has considered in the integrals involved in (30) the beam cross-sections dimensions  $b, h$  for a rectangular cross-section (this however does not restrain the generality of the theory). The notations  $S_x, S_y$  indicate sections respectively orthogonal to the axes  $x, y$  respectively.

This expression of the virtual work of internal forces evidences the following set of classical forces and moments, and generalized forces:

$$\begin{aligned}
N(z) &= \int_S \sigma_{33} ds = ES v'_3 \\
T_x(z) &= \int_S \sigma_{13} ds = GS (v'_1 + \delta a + \delta c), \quad T_y(z) = \int_S \sigma_{23} ds = GS (v'_2 + \delta c + \delta b) \\
Mf_x(z) &= \int_S \xi_1 \sigma_{33} ds = EI_x k'_3, \quad Mf_y(z) = \int_S \xi_2 \sigma_{33} ds = EI_y k'_1 \\
Mt_z(z) &= \int_S (\xi_2 \sigma_{31} - \xi_1 \sigma_{32}) ds = GJ k'_2 \\
q_{11}(x) &= \int_{S_x} \sigma_{11} dx = ES_x \delta a, \quad q_{22}(y) = \int_{S_y} \sigma_{22} dy = ES_y \delta b \\
q_{12}(x) &= \int_{S_x} \sigma_{12} dx = ES_x \delta c, \quad q_{21}(y) = \int_{S_y} \sigma_{12} dy = ES_y \delta c \\
Q_1(z) &= \int_S \xi_1 \sigma_{31} ds = GI \delta a', \quad Q_2(z) = \int_S \xi_2 \sigma_{32} ds = GI \delta b'
\end{aligned} \quad (31)$$

The classical and generalized efforts are introduced in Table 11 below.

Type of	Decriptions	Illustration
---------	-------------	--------------

<b>effort</b>		
Traction-compression  $N(z)$	Classical traction-compression effort (bending line stretch)	
Shear  $T_x(z)$ and $T_y(z)$	The shear effort for Timosheko beams writes: $T_x(z) = \int_s \sigma_{13} ds = GS(\nu_1 + k)$ The generalized shear $T_x(z)$ writes: $T_x(z) = \int_s \sigma_{13} ds$ $= GS(\nu_1 + \delta a + \delta c)$	
Bending  $Mf_x(z)$ and $Mf_y(z)$	Classical bending	
Twist  $Mt_z(z)$	Classical twist  $k = \frac{Mt.l}{J.G}$ twist angle	
Cross-section dilatation  $q_{11}(x)$ and $q_{22}(y)$	Cross-section dilatation representing beam cross-section dilatation and contraction.  The directors remains orthogonal after deformation. This effort is independent of the bending line.	

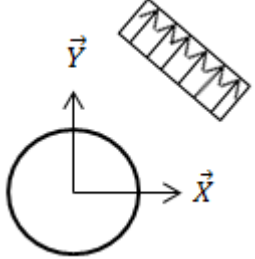
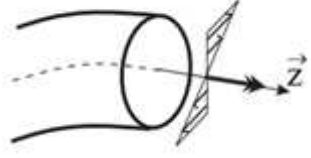
<p>In-plane shear</p> <p><math>q_{12}(x)</math></p>	<p>Cross-section shear describing the change of shape of the beam cross-section.</p> <p>The directors remains normed after deformation.</p>	
<p>Pinching</p> <p><math>Q(z)</math></p>	<p>This effort is similar to the classical twist but it is independent to the length of the beam .</p> <p>The angle of pinching is the angle between <math>a</math> and <math>a'</math> or <math>b</math> and <math>b'</math></p>	

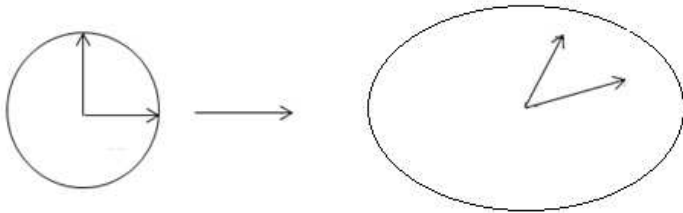
Table 11: interpretation of the beam resultant

## 6. Formulation of the generalized stiffness matrix of the macrobeam

Basing on the expressions of the internal and external virtual work equs (17),(18),(19) the equilibrium equations can then be written:

$$\begin{cases} N + T_x + T_y = \vec{0} \\ Mf_x + Mf_y + Mt_z = \vec{0} \\ q_1 + q_2 + q_{11} + q_{22} = \vec{0} \end{cases} \quad (32)$$

In order to simplify the resolution of the system of equilibrium equations (32), we neglect the terms of pinching by considering that there is not much of non-uniformity in the cross-sectional strains, so we replace equ. (19) by equ. (20). This simplification leads to a classification of beams referring to variables exposed in table 12:

Beam	Variables	Beam and cross section before and after deformation
Macrostrain beam	$v_3, v_1, v_2$ $k_3, k_1, k_2$ $\delta a, \delta b, \delta c$	

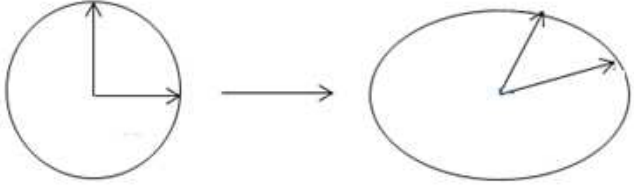
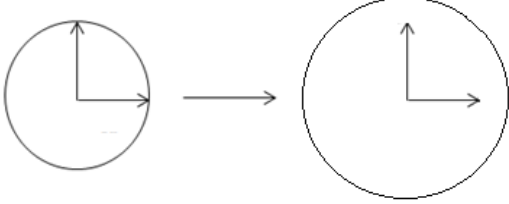
Macroshear beam	$v_3, v_1, v_2$ $k_3, k_1, k_2$ $\delta c$	
Macro dilatation beam	$v_3, v_1, v_2$ $k_3, k_1, k_2$ $\delta a, \delta b$	

Table 12: kinematic variables for the different generalized beam models and their physical meanings

In next section we establish stiffness matrix for the macro dilatation and macroshear beams presented in Table 12.

In this section, we construct the rigidity matrices for the macrostrain, macro dilatation and microshear continua using linear shape functions for the new efforts and relying on the expression of the virtual work of internal forces previously obtained.

Inserting in the expression of the virtual work the previous expressions of the generalized efforts but with a virtual kinematics (indicated by quantities with an overhead hat) delivers the following expression:

$$w_i^* = \left( \int_0^L ES v_3' \hat{v}_3' dz + \int_0^L GS (v_1' + \delta a + \delta c) (\hat{v}_1' + \delta \hat{a} + \delta \hat{c}) dz + \int_0^L GS (v_2' + \delta c + \delta b) (\hat{v}_2' + \delta \hat{b} + \delta \hat{c}) dz \right. \\ \left. + \int_0^L EI_x k_3' \hat{k}_3' dz + \int_0^L EI_y k_1' \hat{k}_1' dz + \int_0^L GJ k_2' \hat{k}_2' dz \right) \quad (33) \\ + \left( \int_0^h ES_x \delta a \delta \hat{a} dx + \int_0^h GS_x \delta c \delta \hat{c} dx \right) + \left( \int_0^b ES_y \delta b \delta \hat{b} dy + \int_0^b GS_y \delta c \delta \hat{c} dy \right)$$

The traction compression stiffness matrix is formulated in the classical way, the interpolation functions must be of class  $C_1$  unlike the interpolation function of the shear which must have the ability to interpolate the second derivative, so it must be of class  $C_2$ . Basing on these approximations the stiffness matrix corresponding to those efforts are next formulated.

The meaning of the various classical and generalized efforts appearing in the expression of the work of internal forces is highlighted in Table 13; the required degree of regularity of the shape functions is indicated in the third column of Table 13 (the notations  $C_1, C_2$  indicate successively the class of first and second continuously derivable functions). The shape functions of the kinematics are introduced in the last column of Table 13; note that kinematic fields with  $C_1$  continuity involve linear shape functions, whereas kinematic quantities with  $C_2$  continuity require quadratic shape functions.

Type of effort	Term in the virtual work of internal forces	Class of test function	Shape functions for the real kinematics
Traction-compression	$\int_0^L ES v_3 \hat{v}_3 dz$	$C_1$	$\zeta_1(z) = 1 - \frac{z}{L}; \zeta_2(z) = \frac{z}{L}$ $V_3(x, t) = \zeta_1(z) V_3^1(t) + \zeta_2(z) V_3^2(t)$
Classical shear and cross-section dilatation	$\left( \int_0^L GS \left( \begin{pmatrix} v_1' + \delta a \\ \hat{v}_1' + \delta \hat{a} \end{pmatrix} \right) dz \right. \\ \left. + \int_0^L EI \delta a' \delta \hat{a}' \right)$	$C_2$	$\zeta_3(z) = \frac{1}{4} \left( 1 - \left( \frac{2z}{L} - 1 \right) \right)^2 \left( 2 + \left( \frac{2z}{L} - 1 \right) \right)$ $\zeta_4(z) = \frac{L}{8} \left( 1 - \left( \frac{2z}{L} - 1 \right) \right) \left( 1 - \left( \frac{2z}{L} - 1 \right)^2 \right)$ $\zeta_5(z) = \frac{1}{4} \left( 1 + \left( \frac{2z}{L} - 1 \right) \right)^2 \left( 2 - \left( \frac{2z}{L} - 1 \right) \right)$ $\zeta_6(z) = \frac{L}{8} \left( 1 + \left( \frac{2z}{L} - 1 \right) \right) \left( -1 + \left( \frac{2z}{L} - 1 \right)^2 \right)$ $v_1(z, t) = \zeta_3(z) v_1^1(t) - \zeta_4(z) v_1^2(t) + \zeta_5(z) v_1^3(t) - \zeta_6(z) v_1^4(t)$ $a(z, t) = -\frac{d\zeta_3}{dz} \zeta_3(z) a^1(t) + \frac{d\zeta_4}{dz} \zeta_4(z) a^2(t) - \frac{d\zeta_5}{dz} \zeta_5(z) a^3(t) + \frac{d\zeta_6}{dz} \zeta_6(z) a^4(t)$

Table 13: mechanical meaning of the introduced generalized efforts

In Table 13 we select the shape functions for the new beam model efforts. We classify these efforts as follows:

- The classical efforts: the traction and twist have the same expression for Timoshenko and the generalized beam.
- The modified efforts: in the new beam model the class of the shape function of the bending effort is  $C_1$  contrary to Timoshenko beam. This difference is caused by the equilibrium equations of each beam: in equation 18, we observe the absence of traction-compression and of shear efforts which affects the boundary conditions and the shape functions.
- The same situation holds for the shear effort, which is class  $C_1$  for Timoshenko model, whereas it is of a higher class  $C_2$  for the generalized beam. For the generalized efforts, we choose the class  $C_1$  for pinching and in plane shear, but as to the cross-section dilatation we combine it with the shear, so we choose the class  $C_2$ .

The expression of the virtual work of internal forces entails after factorization of the kinematic variables written in vector format the following linear relation between the forces (also in vector format) and the kinematic variables, highlighting the stiffness matrix which has a block structure.

We express in equation (34) and (35) successively the linear relations of macrodilataton and macroshear beams:





the torsional modulus, which is identical to the polar moment of inertia of the circular cross-sectional area,  $h$  and  $t$  are depth and width of the beam.

The uniaxial traction, as well as twist modes are inherent to classical beam theories; they are complemented by new expressions of shear, bending and generalized efforts associated to dilatation and in-plane shear which are specific to the introduced generalized beam models.

Note that the rotation of the beam cross-section as well as its rigid body translation which are present in classical beam theories do not appear here, since the stiffness matrix is based on the symmetrical strain tensor which does not include the antisymmetrical part of the displacement gradient. The principal reason for this is that large strains beam mechanics relies on the writing of the finite strain tensor, whereas the displacement field can be directly expressed in linearized beam theories.

## 7. Numerical illustration and validation of the macrobeam model

Two examples are presented below in order to illustrate the proposed enriched beam models; the first example is a tensile test of a nickel beam. We compare the deformations under traction obtained using successively the classical beam theory, the macrodilatation theory and finite element fully resolved simulations. The second example aims at providing an estimate of the overall porosity of microstructured beams of a nickel base material with regular holes, considering different number of holes in order to modify the overall porosity. We shall identify the overall beam porosity from the comparison of the FE results with the macrobeam effective model and relate the macro-dilatation modulus to the overall porosity of the considered domain.

### 7.1 FE validation of the enhanced strain field

We first consider a 2D beam (fig. 4) including as a microstructure a set of circular and symmetric holes distributed regularly within the spatial domain, with the following geometric properties:  $L = 0.15$  m,  $h = 0.015$ , respectively denoting the macrobeam length and width. We choose Nickel as a base material for the beam, the material constants of which selected based on [25], shown in Table 14.



Fig. 4: 2D beam with a regular distribution of periodic holes as a microstructure

Material constants	Value
$\lambda$ [MPa]	122
$\mu$ [MPa]	183
$b_1$ [MPa]	1222
$b_2 = b_3$ [MPa]	1833

$g_1 [MPa]$	-122
$g_2 [MPa]$	-183

Table 14: nickel generalized properties for the base material of the beam adopting the macrodilatation model [25]

Let the beam be fixed at one end and subjected to a transverse concentrated tensile load  $N$  in the positive  $z$ -direction at the other end, with the value of the tensile force  $N= 100$  MPa. We refer to Figure 5 showing the macrobeam and the in-plane ( $z$ - $y$ ) Cartesian coordinates.

We give in Table 15 the expressions of the resulting deformation and dilatation.

	Timoshenko beam	Macrodilatation beam
Deformation	$\varepsilon_{22} = -\frac{1}{2} \frac{\lambda}{\mu(3\lambda + 2\mu)} \sigma_{33}$ $\varepsilon_{33} = \frac{\lambda + \mu}{\mu(3\lambda + 2\mu)} \sigma_{33}$	$\varepsilon_{22} = -\frac{1}{2} \frac{b_1 \lambda^g - g_1^2}{\mu^g (3b_1 \lambda^g + 2b_1 \mu^g - 3g_1^2)} \sigma_{33}$ $\varepsilon_{33} = \frac{b_1 \lambda^g + b_1 \mu^g - g_1^2}{\mu^g (3b_1 \lambda^g + 2b_1 \mu^g - 3g_1^2)} \sigma_{33}$
Dilatation	-	$e_{rr} = -\frac{g_1}{b_1} (\varepsilon_{22} + \varepsilon_{33}), r=1,2$

Table 15: expressions of the deformation and dilatation of the microstructured beam shown in figure 4

The expression of the dilatation term is introduced in the **Appendix 1**; it expresses the dilatation of the directors (the variation of their of norm) attached to every material point of the beam. The values of the in-plane deformations obtained for Timoshenko and microdilatation beams under the applied tensile load are given in Table 16.

Beam model	Deformation		Dilatation	Total deformation	
	$\varepsilon_{33}$	$\varepsilon_{22}$	$e_{22}$	$\varepsilon_{33}$	$\varepsilon_{22} + e_{22}$
Timoshenko	0.25	-0.05	-	0.25	-0.05
Macrodilatation	0.252	-0.05	-0.04	0.25	-0.09

Table 16: Numerical values of the beam cross-section deformation and dilatation

For the macrodilatation we notice that the strain components  $\varepsilon_{33}$  and  $\varepsilon_{22}$  have the same values as those evaluated for the Timoshenko beam. We add the dilatation of the material point  $e_{22}$  given in Table 15 to  $\varepsilon_{22}$  for the macrodilatation beam model in order to evaluate the total deformation; the dilatation accounts here for the local deformation generated by the holes.

We perform in parallel a 2D finite element simulation of the beam which is meant to constitute the reference solution; we extract the strain values (within the  $y$ - $z$  plane)  $\varepsilon_{22}$  and  $\varepsilon_{33}$  around the

beam holes and far from them, the spatial distribution of which being shown in Fig. 5 and Fig. 6 respectively; these values are shown in Table 17.

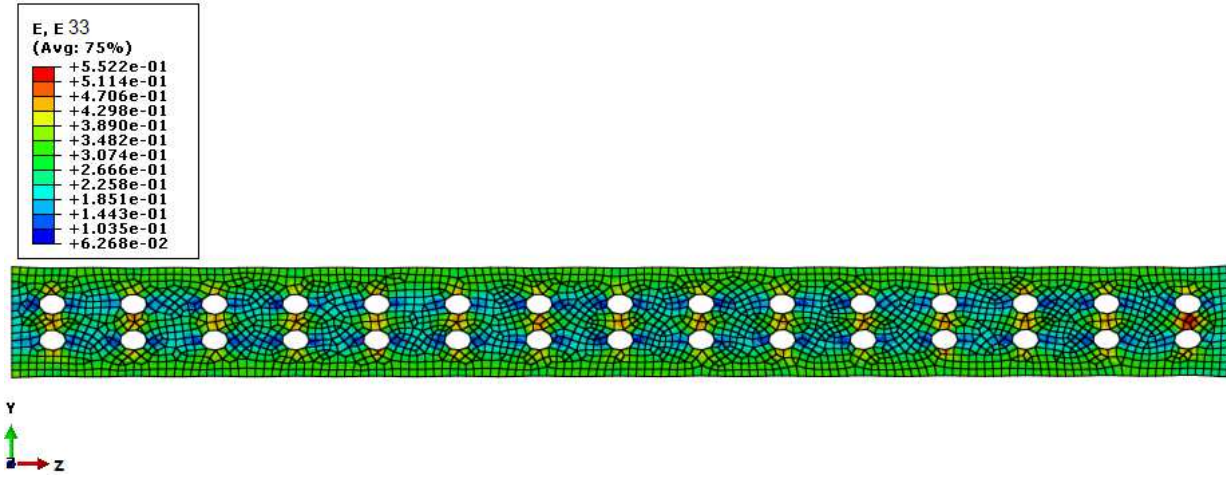


Fig 5: spatial distribution of the local deformation field  $\epsilon_{33}$

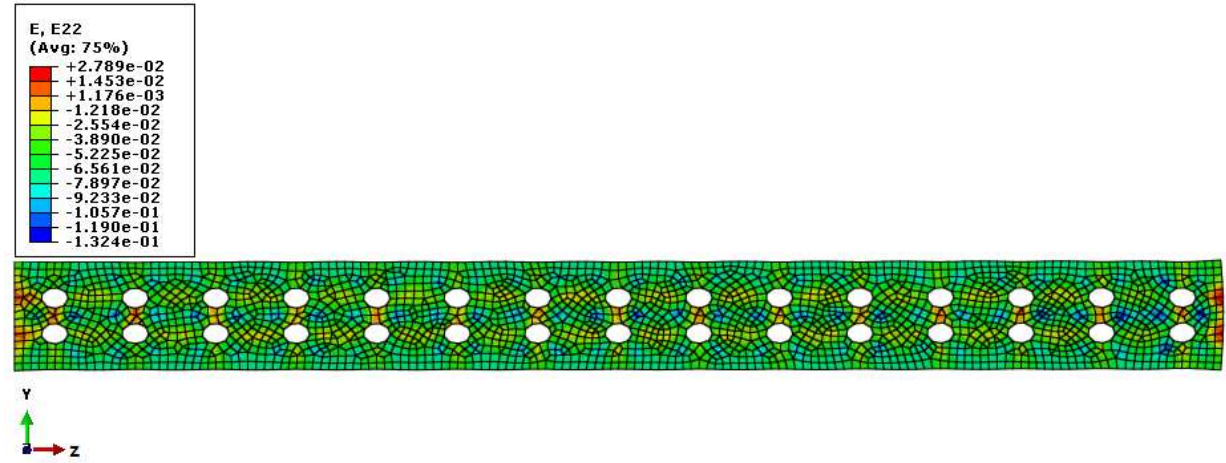


Fig 6: spatial distribution of the local deformation field  $\epsilon_{22}$

Beam model	Deformation		Dilatation	Total deformation	
	$\epsilon_{33}$	$\epsilon_{22}$		$\epsilon_{33}$	$\epsilon_{22} + e_{22}$
Timoshenko	0.25	-0.05	-	0.25	-0.05
Macro dilatation	0.252	-0.05	-0.04	0.25	-0.09

Table 17: FE deformations far and around the holes within the beam

We note that  $\epsilon_{33}$  is positive due to the applied tension, whereas  $\epsilon_{22}$  is negative due to contraction in the transverse direction, by virtue of Poisson's effect. Comparing the deformation values between Tables 16 and 17, it appears that the developed macrodilatation beam predicts the deformation far from the hole, based on the classical strains  $\epsilon_{33}$  and  $\epsilon_{22}$ . Far from the holes, the results are very close to those predicted by finite elements and also by those given by Timoshenko beam model; this follows from the fact that the strain field is not influenced by the

presence of the holes far from them, thus the enriched beam model is in fact not really needed in this case.

Contrary to this, in the vicinity of the holes, the classical beam model is not able to predict the deformation field since  $\varepsilon_{22} = 0.25$  for Timoshenko beam model, which is far from the value  $\varepsilon_{22} = -0.09$  of the reference solution. The strain predicted by the enriched beam model, namely the sum  $\varepsilon_{22} + e_{22} = -0.09$  matches exactly the reference value (Table 17), so that the enriched beam model is shown to determine accurately the deformation around the hole when adding to the classical strain the terms of dilatation (so that the deformation becomes  $\varepsilon_{22} + e_{22}$ ).

The second example developed below provides a comparison between three beams of nickel with different microstructures including different number of holes (16, 20 and 38 holes). The comparison of the postulated macrobeam model with a finite element model will be performed. We shall detect the porosity effect and the relation between the macro-dilatation modulus and the overall porosity.

## 7.2. Porosity effect

Nickel is chosen as a base material for the beam, the material constants of which have been selected based on [25] and are exposed in Table 14. Parameters  $b_1$  and  $g_1$  are supposed to be unknown and will be determined by comparing the prediction of the analytical macrobeam model with 2D finite element simulation results over different microstructured beams incorporating different number of holes (listed in Table 18), these FE results defining the reference solution.

	Number of holes	Porosity
Beam 1	38	0.23
Beam 2	20	0.125
Beam 3	10	0.062

Table 18: porosity and number of holes of each beam

The porosity parameter  $P$  ( $0 \leq P \leq 1$ ) is defined as:

$$P = \frac{\text{volume of holes}}{\text{the total volume of the beam}}$$

Let the beam be fixed at one end and subjected to a transverse concentrated tensile load  $N$  in the positive  $z$ -direction at the other extremity, with the value  $\sigma = 100$  N. The deformations  $\varepsilon_{22}$  and  $\varepsilon_{33}$  are highlighted in Fig. 7, Fig. 8 and Fig. 9; the FE simulations are used to determine the expressions of the macrodilatation moduli  $g_1$  and  $b_1$ .

We recall the expressions of the resulting deformation of a macrodilatation beam:

$$\varepsilon_{22} = -\frac{1}{2} \frac{b_1 \lambda^g - g_1^2}{\mu^g (3b_1 \lambda^g + 2b_1 \mu^g - 3g_1^2)} \sigma_{33}$$

$$\varepsilon_{33} = \frac{b_1 \lambda^g + b_1 \mu^g - g_1^2}{\mu^g (3b_1 \lambda^g + 2b_1 \mu^g - 3g_1^2)} \sigma_{33}$$

Solving the system of equations for the unknown coefficients we find the ratio:

$$\frac{b_1}{\underbrace{g_1^2}_{\gamma}} = \frac{2\varepsilon_{22} + \varepsilon_{33}}{2\lambda\varepsilon_{22} + \lambda\varepsilon_{33} + 2\mu\varepsilon_{22}} \quad (36)$$

The previous system cannot be inverted to provide unique values of the unknown coefficients (since it is singular), so that only their combination through the ratio defined in (36) can be determined. The obtained values of this ratio for each type of beam are computed and presented in Table 19. The deformation around the holes have been averaged within the domain of the representative unit cell of the macrobeam in order to obtain the ratio of the beam macrodilatation coefficients in (36). We note from Table 5 that the deformation around the holes is heterogeneous (showing strong spatial variations), whereas the deformation field far from the holes does not depend on the porosity, as expected (Saint-Venant effect). The spatial distribution of the local strain around the holes computed by FE simulations is shown for the three different beams in fig. 7, 8, 9.

	Number of holes	Deformation far from the holes		Deformation around the holes		$\gamma$
		$\varepsilon_{33}$	$\varepsilon_{22}$	$\varepsilon_{33}$	$\varepsilon_{22}$	
Beam 1	38	0.002	-0.00043	0.004	-0.00096	-0.023
Beam 2	20	0.002	-0.0004	0.004	-0.0011	-0.011
Beam 3	10	0.003	-0.0004	0.0056	-0.0017	-0.0068

Table 19: deformations  $\varepsilon_{33}$  and  $\varepsilon_{22}$  and  $\gamma$  for the different microstructured beams including holes

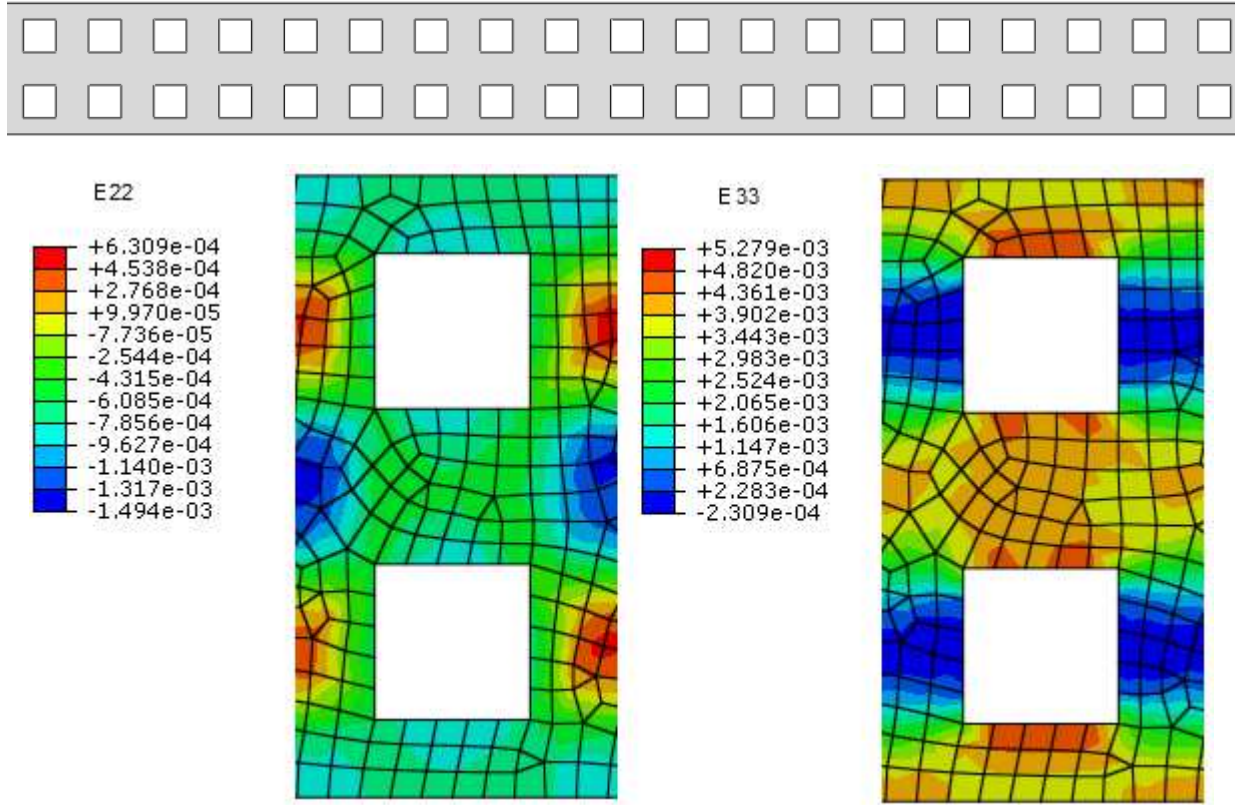


Fig. 7: 2D FE beam with 38 holes under simple traction. Left: deformation distribution  $\varepsilon_{22}$ .  
Right: deformation distribution  $\varepsilon_{33}$



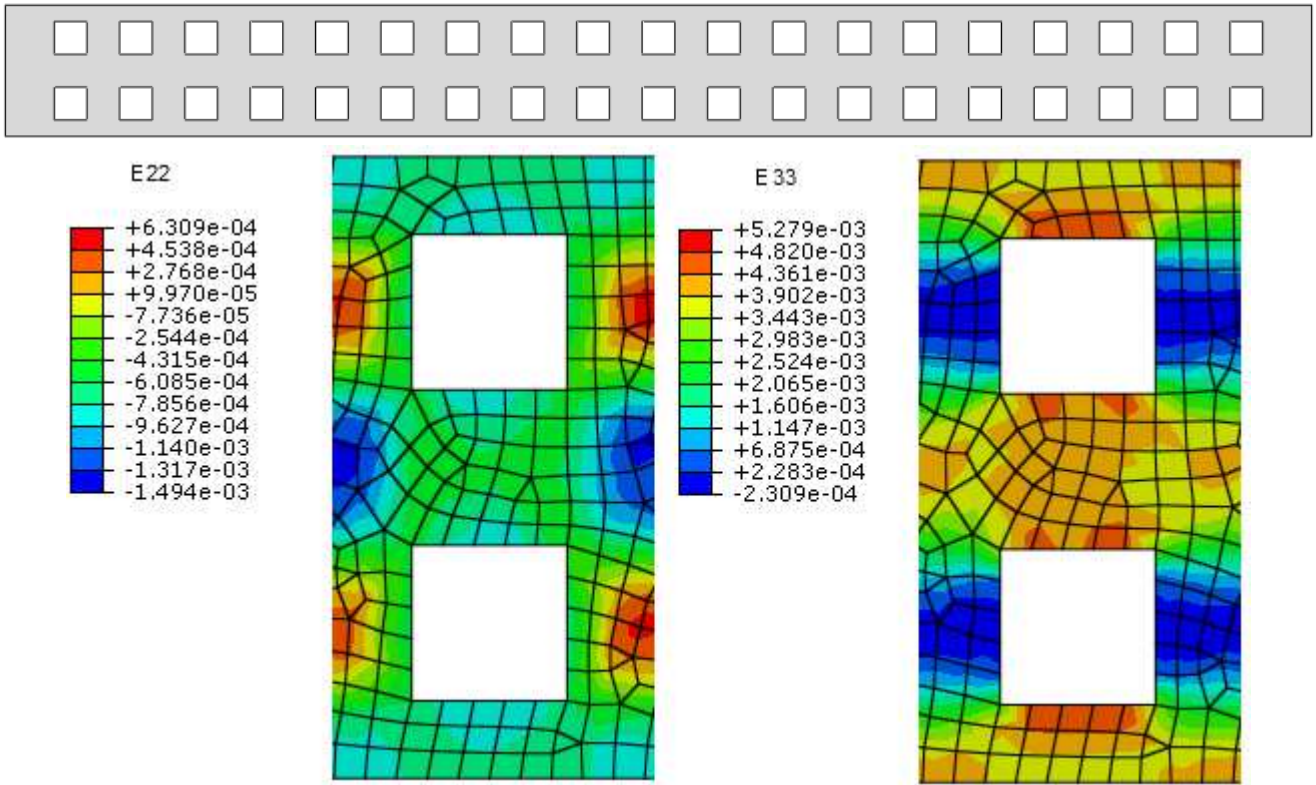


Fig 8: 2D FE beam with 20 holes under simple traction. Left: deformation distribution  $\epsilon_{22}$  . Right: deformation distribution  $\epsilon_{33}$

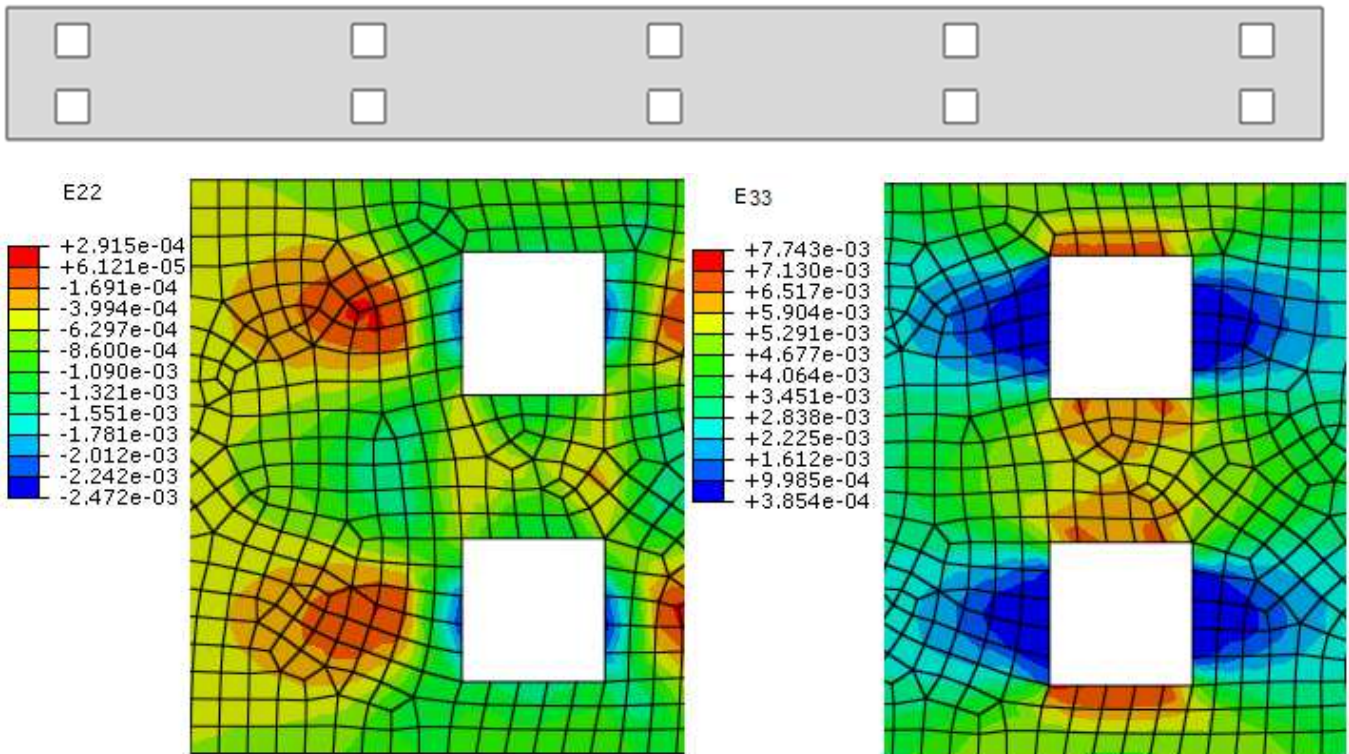


Fig 9: 2D FE beam with 10 holes under simple traction. Left: deformation distribution  $\epsilon_{22}$  . Right: deformation distribution  $\epsilon_{33}$



Table 19 and equ. (35) show that the ratio  $\gamma := \frac{g_1^2}{b_1}$  does not depends on the stress  $\sigma$  but it depends on the number of holes.

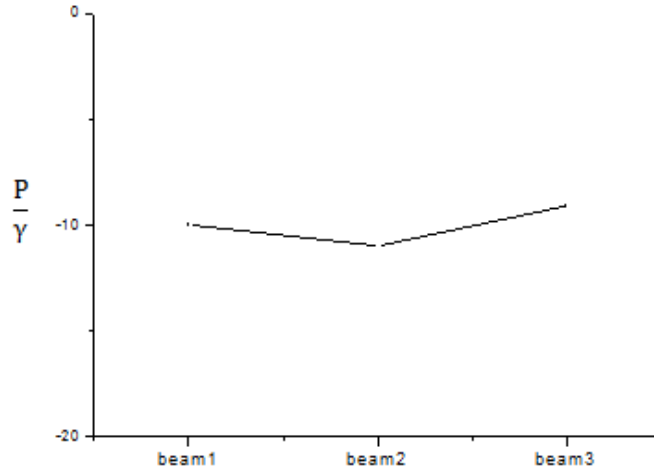


Fig. 10. Values of the ratio  $\frac{P}{\gamma}$  for the different microstructured beams

Figure 10 shows that the coefficient  $\gamma$  is strongly correlated to the porosity since the ratio  $\frac{P}{\gamma}$  is nearly constant for the different considered microstructures, thus it provides a quantitative measure of the overall porosity. The identification of the coefficients of the different enriched beam models constructed in this contribution is an important issue that will be addressed in future contributions.

## 8. Conclusion

Beam theories are all based on simplifying assumptions, since a full 3D model including all deformation modes in the context of finite strains is still challenging nowadays and no unitary view yet exists. None of the classical beam theories is able incorporate non-classical effects such as warping, or out- and in-plane deformations; these phenomena are important for thick beams undergoing large motions, in applications involving complex yarns subjected to transverse compaction, like electric wires, multifilamentary structures in technical textiles, submarine cables, or ligaments and muscles in the context of biomechanics.

The main objective of this work is to take into account the section dilatation and the in-plane shear that develop within thick beams in a finite strains context. As a novel aspect, enriched beam model called macrodilatation, macroshear, and macrostrain beam models have been constructed on the basis of generalized beam theories but with a more condensed kinematics, assuming a uniform hyperstress tensor; this leads to new macro-continua, and their constitutive law enters the generalized efforts for the developed beam models.

The choice of the adequate extended continuum for a given beam depends on its macroscopic deformation mechanisms. As a result, the developed beam models include modified material parameters (the tensile, shear and bulk moduli for an isotropic beam) involving additional microstructural parameters. These macrobeam models better describe the in plane-shear and

dilatation of the beam sections along the mean line in comparison to classical beam theories; this has been illustrated by evaluating the local strain field in the vicinity of holes within a beam subjected to a tensile loading and identifying parameters of the macrodilatation beam model by comparing with fully resolved FE simulations. The macrodilatation parameters intervene via a combination of them giving an estimate of the average porosity.

This work on enriched beam models constitutes the basis for the homogenization of generalized beam lattices towards microstretch, microstrain, microshear and micromorphic continua, extending the micropolar effective substitution continuum which has been developed for network materials [23, 24]. The identification of the new material coefficients of the enriched beam models constructed in this work is a long-term objective that will deserve future contributions.

## References

- [1] Timoshenko SP. On the transverse vibrations of bars of uniform cross-section. The London, Edinburgh, and Dublin Philosophical Magazine and Journal of Science 1922; 43(253), 125-131.
- [2] Timoshenko SP., Gere J. M. Theory of Elastic Stability. Dover Publications, 2nd edition, 1961.
- [3] Euler L. De curvis elasticis. 1744; In: Methodus Inveniendi Lineas Curvas Maximi Minimive Proprietate Gaudentes, Sive Solutio Problematis Isoperimetrici Lattissimo Sensu, Accepti. Bousquet.
- [4] Love AEH. On the small free vibrations and deformations of elastic shells, Philosophical trans. of the Royal Society (London) 1888; Série A, N° 17 p. 491–549.
- [5] Antman S.S. Nonlinear problems of elasticity. Springer-Verlag; 1995.
- [6] Kumar A., Mukherjee S. A geometrically exact rod model including in-plane cross-sectional deformation. Journal of Applied Mechanics ; 2011, 78(1).
- [7] Ballard P., Millard A. Poutres et arcs élastiques. Editions Ecole Polytechnique; 2009.
- [8] Attia H. Modélisation multi-échelles du comportement mécanique des câbles textiles. 2015. PhD thesis, Ecole Centrale Paris. Français. NNT : 2015ECAP0018.
- [9] Rubin M., Mordecai B. Cosserat theories: shells, rods and points. Vol.79. Springer Science & Business Media; 2013.
- [10] Eringen A.C., Suhbi E.S. Nonlinear theory of simple micro-elastic solids. Int. J. Engng Sci.; 1964; 2.2 (164): 189-203.
- [11] Forest, S. Sievert, S. Nonlinear microstrain theories. Int. J. Solids Struct.; 2006;43.24, 7224-7245.
- [12] Eringen, AC. Theory of thermo-microstretch elastic solids. Int. J. Engng Sci.; 28.12 1291-1301, 1990.
- [13] Eringen AC., Suhubi E.S. Nonlinear theory of simple micro-elastic solids—I. Int. J. Eng. Sci.; 1964, 2(2), pp. 189–203.
- [14] Cosserat E., Cosserat F. Theorie des Corps Deformables, A. Hermann, Paris; 1909.
- [15] Günther W. Zur statik und kinematik des cosseratschen kontinuums. Abh. Braunschweig; 1958 Wiss. Ges, 10(213), p. 1.
- [16] Mindlin R.D., Micro-structure in linear elasticity. Arch. Ration. Mech. Anal.; 1964, 16(1), pp. 51–78.
- [17] Cowin S.C., Nunziato J.W. Linear elastic materials with voids. J. Elast.; 1983, 13(2), p. 125–147.
- [18] Forest S., Sievert R. Nonlinear microstrain theories. Int. J. Solids Struct.; 2006 43(24), p. 7224–7245.
- [19] Kirchner N., and Steinmann P. Mechanics of extended continua: modeling and simulation of elastic microstretch materials. Comput. Mech.; 2007, 40(4), pp. 651–666.
- [20] Ramézani H., Steeb H., Jeong J. Analytical and numerical studies on Penalized Micro-Dilatation (PMD) theory: Macro-micro link concept. Eur. J. Mech. A Sol., 2012, 34, p. 130–148.

- [21] Jeong J., Sardini P., Ramézani H., Siitari-Kauppi M., Steeb H., Modeling of the induced chemo-mechanical stress through porous cement mortar subjected to CO<sub>2</sub>: Enhanced micro-dilatation theory and 14C-PMMA method. *Comput. Mater. Sci.*; 2013, 69(0), pp. 466–480.
- [22] Thureau, N. Sur la modélisation du tissu cardiaque comme un milieu à microdilatation: une investigation numérique. PhD Thesis, Université de Lorraine, 2014.
- [23] Dos Reis F., Ganghoffer J.F. Construction of micropolar models from lattice homogenization. *Computers Struct.*; 2012, 112-113, p. 354-363.
- [24] Goda I., Assidi M., Ganghoffer J.F. A micropolar constitutive model of cancellous bone from discrete homogenization. *Computer Methods in Biomechanics and Biomedical Engineering*; 2012, 16:87-108. doi: 10.1016/j.jmbbm.2012.07.012.
- [25] Neff, P., & Forest, S. (2007). A geometrically exact micromorphic model for elastic metallic foams accounting for affine microstructure. *Modelling, existence of minimizers, identification of moduli and computational results. Journal of Elasticity*, 87(2-3), 239-276.
- [26] Gruttmann, F., and W. Wagner. "Shear correction factors in Timoshenko's beam theory for arbitrary shaped cross-sections." *Computational Mechanics* 27.3 (2001): 199-207.
- [27] El Fatmi R 2002 On the structural behavior and the Saint Venant solution in the exact beam theory: application to laminated composite beams. *Computers & Structures*, 80(16–17), 1441–1456.
- [28] Berdichevsky VL, Armanios E, and Badir, A., 1992. Theory of anisotropic thin-walled closed cross-section beams. *Composites Engineering*, 2(5–7), 411–432.
- [29] Carrera E and Giunta G 2010 Refined beam theories based on a unified formulation. *International Journal of Applied Mechanics*, 2(1), 117–143.

## Appendix 1: construction of the macrostretch continuum

The constitutive equations of the microdilatation continuum include the following expressions of the stress, relative stress and hyperstress tensors, given in component form as:

$$\sigma_{kl} = (\lambda^g \varepsilon_{rr} + g_1 e_{rr}) \delta_{kl} + 2\mu^g \varepsilon_{kl}$$

$$s_{kl} = (g_1 \varepsilon_{rr} + b_1 e_{rr}) \delta_{kl}$$

$$S_m = \tau_{12} e_{rr,m}$$

The Cauchy stress, the relative stress and the hyperstress tensors satisfy the static balance equations for the micromorphic medium, written in index notation:

$$\sigma_{kl,l} = 0$$

$$S_{klm,m} + \sigma_{kl} - s_{kl} = 0$$

In these continua, we will suppose that the hyper-stress is uniform in the solid body [22], thus its gradient also vanishes; we can then extract the expressions of the relative deformation from the previous balance equation:

$$e_{rr} = -\frac{g_1}{b_1}$$

Inserting  $e_{rr}$  in the previous expression of the stress tensor delivers the constitutive equation of the macrostrain continuum:

$$\sigma_{kl} = \left( \lambda^g - \frac{g_1^2}{b_1} \right) \varepsilon_{rr} \delta_{kl} + 2\mu^g \varepsilon_{kl}$$

We determinate the expressions of the other macrocontinua with the same method.

## Appendix 2: determination of the small strains tensor

The small strains tensors are obtained by linearizing the corresponding micromorphic beam large strain tensors in the previous Table. The pure deformation tensor in the polar decomposition of the transformation gradient simplifies to the identity tensor, whereas it is generalized in the

present enriched beam model to  $\mathbf{U} = \begin{bmatrix} a & c & 0 \\ c & b & 0 \\ 0 & 0 & 1 \end{bmatrix}$ , which gives after linearization

$$\mathbf{U} \equiv \begin{pmatrix} 1+\delta a & \delta c & 0 \\ \delta c & 1+\delta b & 0 \\ 0 & 0 & 1 \end{pmatrix} = \mathbf{I} + \boldsymbol{\psi} \Rightarrow \boldsymbol{\psi} = \begin{pmatrix} \delta a & \delta c & 0 \\ \delta c & \delta b & 0 \\ 0 & 0 & 0 \end{pmatrix} = \begin{pmatrix} \psi_{11} & \psi_{12} & 0 \\ \psi_{12} & \psi_{22} & 0 \\ 0 & 0 & 0 \end{pmatrix}$$

with  $\boldsymbol{\psi}$  therein incremental pure deformation tensor. The rotation tensor is further linearized as

$$\mathbf{R} \cong \mathbf{I} + \mathbf{w}, \quad \mathbf{w} + \mathbf{w}^T = \mathbf{0}$$

introducing therein the antisymmetrical rotation tensor  $\mathbf{w}$ . This entails the antisymmetrical tensor

$$\mathbf{K} := \mathbf{R}^T \cdot \mathbf{R}' \cong \mathbf{w}' = \begin{pmatrix} 0 & -k_2 & k_3 \\ k_2 & 0 & -k_1 \\ -k_3 & k_1 & 0 \end{pmatrix}$$

We further linearize the vector  $\mathbf{v} \equiv \begin{pmatrix} 1+w_1 \\ 1+w_2 \\ 1+w_3 \end{pmatrix}$ , considering an equal cross-section dilatation.

We next linearize all components involved in the Lagrangian finite strain tensor

$$\mathbf{E} = \frac{1}{2} \underbrace{\begin{pmatrix} (\mathbf{d}_1 \cdot \mathbf{d}_1) - 1 & (\mathbf{d}_1 \cdot \mathbf{d}_2) & (\mathbf{d}_1 \cdot \mathbf{r}') + \xi_2(\mathbf{d}_1 \cdot \mathbf{d}_2') + \xi_1(\mathbf{d}_1 \cdot \mathbf{d}_1') \\ (\mathbf{d}_1 \cdot \mathbf{d}_2) & (\mathbf{d}_2 \cdot \mathbf{d}_2) - 1 & (\mathbf{d}_2 \cdot \mathbf{r}') + \xi_1(\mathbf{d}_2 \cdot \mathbf{d}_1') + \xi_2(\mathbf{d}_2 \cdot \mathbf{d}_2') \\ (\mathbf{d}_1 \cdot \mathbf{r}') + \xi_2(\mathbf{d}_1 \cdot \mathbf{d}_2') + \xi_1(\mathbf{d}_1 \cdot \mathbf{d}_1') & (\mathbf{d}_2 \cdot \mathbf{r}') + \xi_1(\mathbf{d}_2 \cdot \mathbf{d}_1') + \xi_2(\mathbf{d}_2 \cdot \mathbf{d}_2') & (\mathbf{r}' \cdot \mathbf{r}') + \xi_1(\mathbf{r}' \cdot \mathbf{d}_1') - \xi_2(\mathbf{r}' \cdot \mathbf{d}_2') - 1 \end{pmatrix}}_{\text{Antmann formulation}}$$

We shall use the following intermediate results:

$$\mathbf{d}_\alpha = \mathbf{R} \cdot \mathbf{U} \cdot \mathbf{e}_\alpha \Rightarrow \mathbf{d}'_\alpha = (\mathbf{R}' \cdot \mathbf{U} + \mathbf{R} \cdot \mathbf{U}') \cdot \mathbf{e}_\alpha$$

$$\mathbf{U}^2 \cong \mathbf{I} + 2\boldsymbol{\psi}$$

$$\mathbf{R}^T \cdot \mathbf{R}' := \mathbf{w}' := \mathbf{K}$$

$$\mathbf{R}^T \cdot \mathbf{r}' = \mathbf{v} \equiv \begin{pmatrix} 1+w_1 \\ 1+w_2 \\ 1+w_3 \end{pmatrix}$$

This entails the following products and their linearization:

$$\mathbf{d}_1 \cdot \mathbf{d}_1 = \mathbf{e}_1 \cdot \mathbf{U}^2 \cdot \mathbf{e}_1 \equiv \mathbf{e}_1 \cdot (\mathbf{I} + 2\boldsymbol{\psi}) \cdot \mathbf{e}_1 = 1 + \psi_{11}, \quad \mathbf{d}_1 \cdot \mathbf{d}_2 \equiv \psi_{12}, \quad \mathbf{d}_2 \cdot \mathbf{d}_2 = \mathbf{e}_2 \cdot \mathbf{U}^2 \cdot \mathbf{e}_2 \equiv \mathbf{e}_2 \cdot (\mathbf{I} + 2\boldsymbol{\psi}) \cdot \mathbf{e}_2 = 1 + \psi_{22}$$

$$\mathbf{d}_1 \cdot \mathbf{r}' = (\mathbf{R} \cdot \mathbf{U} \cdot \mathbf{e}_1)^T \cdot \mathbf{r}' = \mathbf{e}_1 \cdot \mathbf{U} \cdot \mathbf{v} \equiv \mathbf{e}_1 \cdot (\mathbf{I} + 2\boldsymbol{\psi}) \cdot \mathbf{v} \equiv 1 + w_1 + \psi_{11} + \psi_{12} + \psi_{11}w_1 + \psi_{12}w_2$$

$$\mathbf{d}_2 \cdot \mathbf{r}' = (\mathbf{R} \cdot \mathbf{U} \cdot \mathbf{e}_2)^T \cdot \mathbf{r}' = \mathbf{e}_2 \cdot \mathbf{U} \cdot \mathbf{v} \equiv \mathbf{e}_2 \cdot (\mathbf{I} + 2\boldsymbol{\psi}) \cdot \mathbf{v} \equiv 1 + w_2 + \psi_{12} + \psi_{22} + \psi_{12}w_1 + \psi_{22}w_2$$

$$\mathbf{d}_1 \cdot \mathbf{d}'_1 = (\mathbf{R} \cdot \mathbf{U} \cdot \mathbf{e}_1)^T \cdot (\mathbf{R}' \cdot \mathbf{U} + \mathbf{R} \cdot \mathbf{U}') \cdot \mathbf{e}_1 = \mathbf{e}_1 \cdot (\mathbf{U} \cdot \mathbf{R}^T \cdot \mathbf{R}' \cdot \mathbf{U} + \mathbf{U} \cdot \mathbf{U}') \cdot \mathbf{e}_1 = \mathbf{e}_1 \cdot (\mathbf{U} \cdot \mathbf{K} \cdot \mathbf{U} + \mathbf{U} \cdot \mathbf{U}') \cdot \mathbf{e}_1 \equiv$$

$$\mathbf{e}_1 \cdot ((\mathbf{I} + \boldsymbol{\psi}) \cdot \mathbf{K} \cdot (\mathbf{I} + \boldsymbol{\psi}) + (\mathbf{I} + \boldsymbol{\psi}) \cdot \boldsymbol{\psi}') \cdot \mathbf{e}_1 \equiv \mathbf{e}_1 \cdot (\mathbf{K} + \boldsymbol{\psi} \cdot \mathbf{K} + \mathbf{K} \cdot \boldsymbol{\psi}) \cdot \mathbf{e}_1 + \psi'_{11}$$

$$\boldsymbol{\psi} \cdot \mathbf{K} = \begin{pmatrix} k_2 \delta c & -k_2 \delta a & k_3 \delta a - k_1 \delta c \\ k_2 \delta b & -k_2 \delta c & k_3 \delta c - k_1 \delta b \\ 0 & 0 & 0 \end{pmatrix}, \quad \mathbf{K} \cdot \boldsymbol{\psi} = \begin{pmatrix} -k_2 \delta c & -k_2 \delta b & 0 \\ k_2 \delta a & k_2 \delta c & 0 \\ -k_3 \delta a + k_1 \delta c & k_3 \delta c + k_1 \delta b & 0 \end{pmatrix}$$

$$\Rightarrow \boldsymbol{\psi} \cdot \mathbf{K} + \mathbf{K} \cdot \boldsymbol{\psi} = \begin{pmatrix} 0 & -k_2(\delta b + \delta a) & k_3 \delta a - k_1 \delta c \\ k_2(\delta a + \delta b) & 0 & k_3 \delta c - k_1 \delta b \\ -k_3 \delta a + k_1 \delta c & -k_3 \delta c + k_1 \delta b & 0 \end{pmatrix} \text{ antisymmetrical}$$

$$\rightarrow \mathbf{d}_1 \cdot \mathbf{d}'_1 \equiv K_{11} + \mathbf{e}_1 \cdot (\boldsymbol{\psi} \cdot \mathbf{K} + \mathbf{K} \cdot \boldsymbol{\psi}) \cdot \mathbf{e}_1 + \psi'_{11} \equiv \psi'_{11}$$

$$\mathbf{d}_1 \cdot \mathbf{d}'_2 = (\mathbf{R} \cdot \mathbf{U} \cdot \mathbf{e}_1)^T \cdot (\mathbf{R}' \cdot \mathbf{U} + \mathbf{R} \cdot \mathbf{U}') \cdot \mathbf{e}_2 = \mathbf{e}_1 \cdot (\mathbf{U} \cdot \mathbf{K} \cdot \mathbf{U} + \mathbf{U} \cdot \mathbf{U}') \cdot \mathbf{e}_2 \equiv K_{12} + \mathbf{e}_1 \cdot (\boldsymbol{\psi} \cdot \mathbf{K} + \mathbf{K} \cdot \boldsymbol{\psi}) \cdot \mathbf{e}_2 + \psi'_{12}$$

$$\equiv -k_2 + w'_{12} - k_2(\psi_{22} + \psi_{11})$$

$$\mathbf{d}'_1 \cdot \mathbf{d}_2 = \mathbf{d}_2 \cdot \mathbf{d}'_1 = (\mathbf{R} \cdot \mathbf{U} \cdot \mathbf{e}_2)^T \cdot (\mathbf{R}' \cdot \mathbf{U} + \mathbf{R} \cdot \mathbf{U}') \cdot \mathbf{e}_1 = \mathbf{e}_2 \cdot (\mathbf{U} \cdot \mathbf{K} \cdot \mathbf{U} + \mathbf{U} \cdot \mathbf{U}') \cdot \mathbf{e}_1$$

$$\equiv K_{21} + \mathbf{e}_2 \cdot (\boldsymbol{\psi} \cdot \mathbf{K} + \mathbf{K} \cdot \boldsymbol{\psi}) \cdot \mathbf{e}_1 + \psi'_{21} \equiv k_2 + w'_{12} + k_2(\psi_{11} + \psi_{22})$$

$$\mathbf{d}_2 \cdot \mathbf{d}'_2 \equiv K_{22} + \mathbf{e}_2 \cdot (\boldsymbol{\psi} \cdot \mathbf{K} + \mathbf{K} \cdot \boldsymbol{\psi}) \cdot \mathbf{e}_2 + \psi'_{22} \equiv \psi'_{22}$$

$$\mathbf{r}' \cdot \mathbf{d}_1' = (\mathbf{R}^T \cdot \mathbf{r}') \cdot (\mathbf{R}^T \cdot \mathbf{d}_1') = \mathbf{v} \cdot (\mathbf{R}^T \cdot \mathbf{d}_1') = \mathbf{v} \cdot (\mathbf{R}^T \cdot (\mathbf{R}' \cdot \mathbf{U} + \mathbf{R} \cdot \mathbf{U}') \cdot \mathbf{e}_1) = \mathbf{v} \cdot \mathbf{K} \cdot \mathbf{U} \cdot \mathbf{e}_1 + \mathbf{v} \cdot \mathbf{U}' \cdot \mathbf{e}_1 \equiv \mathbf{v} \cdot \mathbf{K} \cdot (\mathbf{I} + \boldsymbol{\psi}) \cdot \mathbf{e}_1 + \mathbf{v} \cdot \boldsymbol{\psi}' \cdot \mathbf{e}_1$$

$$\equiv \mathbf{v} \cdot \mathbf{K} \cdot \mathbf{e}_1 + \mathbf{v} \cdot \mathbf{K} \cdot \boldsymbol{\psi} \cdot \mathbf{e}_1 + \mathbf{v} \cdot \boldsymbol{\psi}' \cdot \mathbf{e}_1 \equiv k_2 - k_3 + w_2 k_2 - w_3 k_3 + \psi_{11}(-k_2 k_3) + \psi_{12}(k_1 - k_2) + w'_1 \psi_{11} + w'_2 \psi_{12}$$

$$\mathbf{r}' \cdot \mathbf{d}_2' = \mathbf{v} \cdot \mathbf{K} \cdot \mathbf{U} \cdot \mathbf{e}_2 + \mathbf{v} \cdot \mathbf{U}' \cdot \mathbf{e}_2 \equiv \mathbf{v} \cdot \mathbf{K} \cdot (\mathbf{I} + \boldsymbol{\psi}) \cdot \mathbf{e}_2 + \mathbf{v} \cdot \boldsymbol{\psi}' \cdot \mathbf{e}_2 \equiv \mathbf{v} \cdot \mathbf{K} \cdot \mathbf{e}_2 + \mathbf{v} \cdot \mathbf{K} \cdot \boldsymbol{\psi} \cdot \mathbf{e}_2 + \mathbf{v} \cdot \boldsymbol{\psi}' \cdot \mathbf{e}_2 \equiv$$

$$k_1 - k_2 - w_2 k_2 + w_1 k_1 - k_2 \psi_{22} + k_2 \psi_{12} + k_3 \psi_{12} + k_1 \psi_{22} + w'_1 \psi_{12} + w'_2 \psi_{22}$$

$$\mathbf{r}' \cdot \mathbf{r}' = (\mathbf{R}^T \cdot \mathbf{r}') \cdot (\mathbf{R}^T \cdot \mathbf{r}') = \mathbf{v} \cdot \mathbf{v} \equiv 1 + 2(w_1 + w_2 + w_3)$$

$$\Rightarrow \mathbf{r}' \cdot \mathbf{r}' + \xi_1(\mathbf{r}' \cdot \mathbf{d}_1') - \xi_2(\mathbf{r}' \cdot \mathbf{d}_2') - 1 \equiv 2(w_1 + w_2 + w_3) +$$

$$\xi_1(k_2 - k_3 + w_2 k_2 - w_3 k_3 + \psi_{11}(-k_2 k_3) + \psi_{12}(k_1 - k_2) + w'_1 \psi_{11} + w'_2 \psi_{12})$$

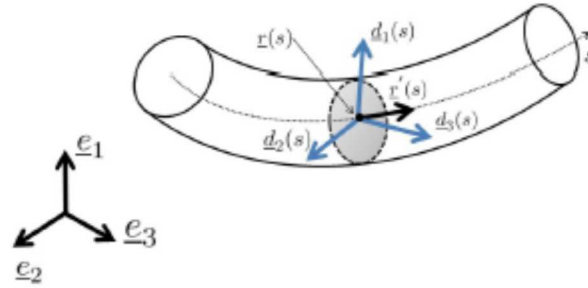
$$- \xi_2(-k_2 + k_1 - w_1 k_2 + w_3 k_1 - k_2 v_1 \psi_{22} + k_2 v_2 \psi_{12} + k_3 v_3 \psi_{12} + k_1 v_3 \psi_{22}) \equiv 2w_3$$

Using previous developments delivers the linearized strain tensor:

$$\bar{\mathbf{E}} = \frac{1}{2} \begin{bmatrix} \psi_{11} & \psi_{12} & 1 + w_1 + \psi_{11} + \psi_{12} - \xi_2 k_2 + \xi_1 \psi'_{11} \\ \psi_{21} & \psi_{22} & 1 + w_2 + \psi_{12} + \psi_{22} + \xi_1 k_2 + \xi_2 \psi'_{22} \\ - & - & 2w_3 + \xi_1(k_2 - k_3) + \xi_2(k_1 - k_2) \end{bmatrix}$$

with the linearized quantities therein  $\psi_{11} = \delta a$ ,  $\psi_{22} = \delta b$ ,  $\psi_{12} = \delta c$ .

# Graphical abstract



Cross-section of a beam with the three directors in the deformed configuration

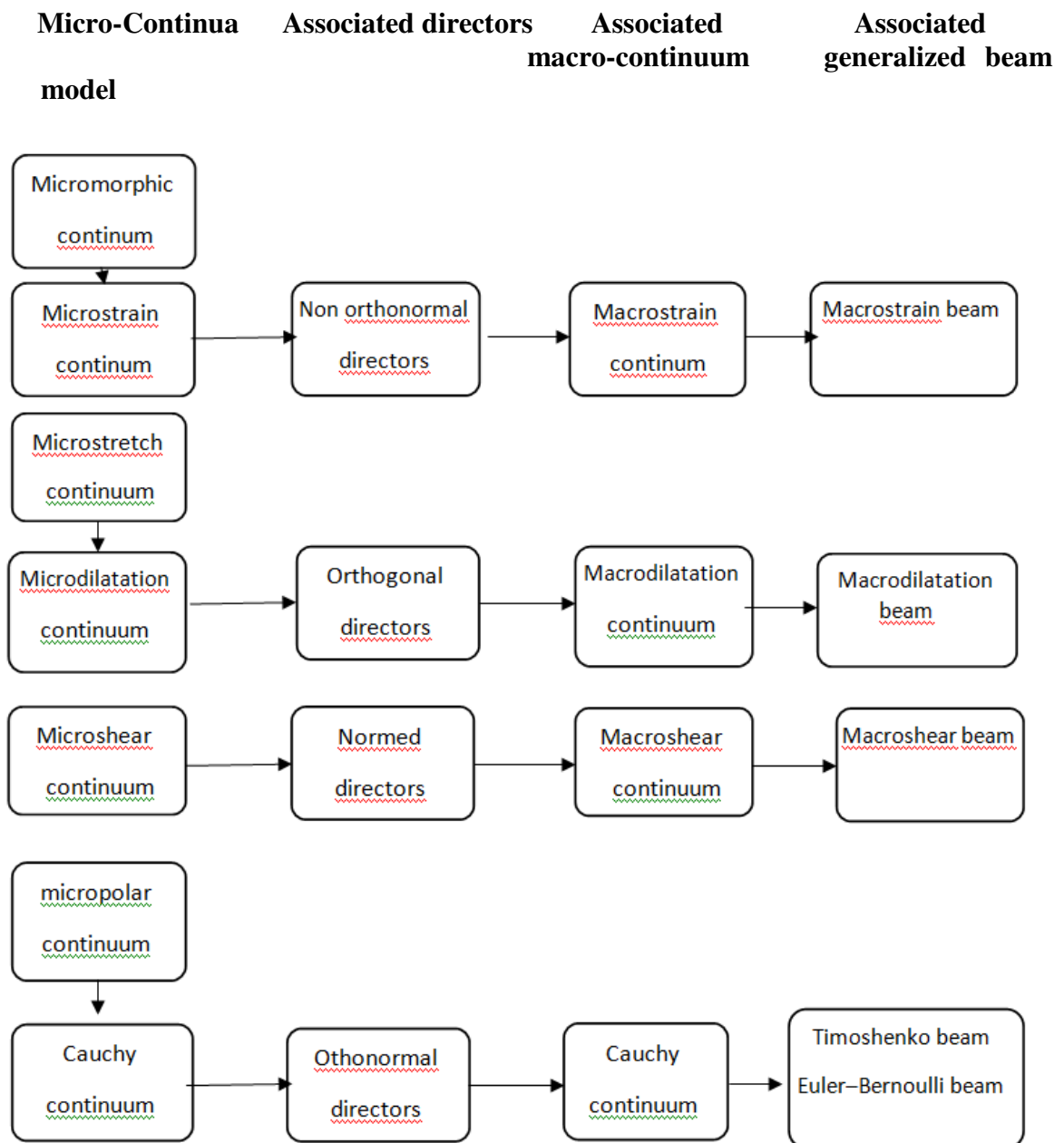
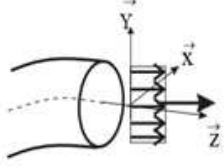
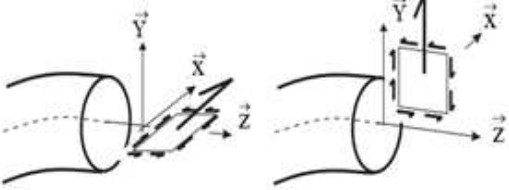
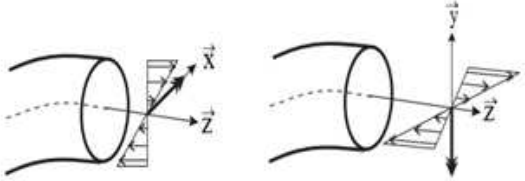
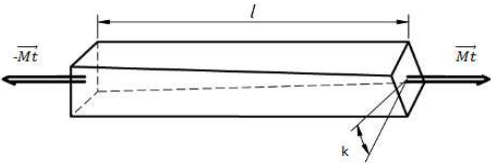
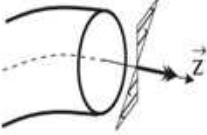
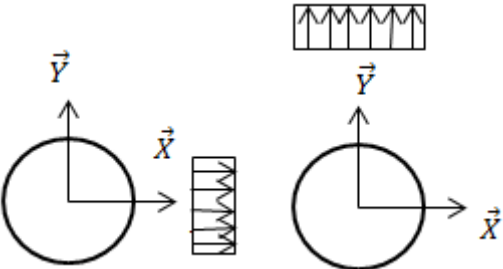
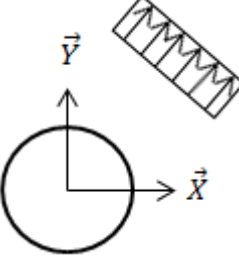


Table 6: Classification of beam models based on reduction of the microcontinua

Type of effort	Description	Illustration
Traction-compression $N(z)$	Classical traction-compression effort (bending line stretch)	
Shear $T_x(z)$ and $T_y(z)$	The shear effort for Timosheko beams writes: $T_x(z) = \int_s \sigma_{13} ds = GS(v_1 + k)$ The generalized shear $T_x(z)$ writes: $T_x(z) = \int_s \sigma_{13} ds = GS(v_1 + \delta a + \delta c)$	
Bending $Mf_x(z)$ and $Mf_y(z)$	Classical bending	 $Mf_x(z)$ $Mf_y(z)$
Twist $Mt_z(z)$	Classical twist  $k = \frac{Mt.l}{J.G} \text{ twist angle}$	
Cross-section dilatation $C_{11}(x)$ and $C_{22}(y)$	Cross-section dilatation representing beam cross-section dilatation and contraction. The directors remains orthogonal after deformation. This effort is independent of the bending line.	
In-plane shear $C_{12}(x)$	Cross-section shear describing the change of shape of the beam cross-section. The directors remains normed after deformation.	



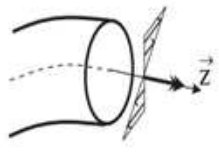
Pinching $D(z)$	This effort is similar to the classical twist but it is independent to the length of the beam .  The angle of pinching is the angle between $a$ and $a'$	
--------------------	--	---

Table 11: interpretation of the beam resultants for the macrobeam continuum